An electrical network model for computing current distribution in a spirally wound lithium ion cell

by
Somani Patnaik
S.B. EECS, M.I.T., 2011

Submitted to the Department of Electrical Engineering and Computer Science
in Partial Fulfillment of the Requirements for the Degree of
Master of Engineering in Electrical Engineering and Computer Science
at the Massachusetts Institute of Technology
September, 2012

Author:

Department of Electrical Engineering and Computer Science, September 7, 2012

Certified by:

Jing Kong, Associate Professor, EECS, Thesis Supervisor September 7, 2012

Certified by:

Jake Christensen, Principal Engineer, Robert Bosch LLC, Thesis Co-Supervisor
September 7, 2012

Accepted by:

Prof. Dennis M. Freeman, Chairman, Masters of Engineering Thesis Committee

An electrical network model for computing current distribution in a spirally wound lithium ion cell

by
Somani Patnaik
Submitted to the
Department of Electrical Engineering and Computer Science

September 7, 2012
In Partial Fulfillment of the Requirements for the Degree of
Master of Engineering in Electrical Engineering and Computer Science

ABSTRACT

Lithium ion batteries are the most viable option for electric vehicles but they still have significant limitations. Safety of these batteries is one of the concerns that need to be addressed when they are used in mainstream vehicles, because of heating issues that may lead to thermal runaway. This work aims at supplementing the existing electrochemical heat distribution model of a spirally wound lithium ion battery with an electrical network that can model the heat losses due to electric resistances of the current collectors. The developed electrical network model is used to calculate the current and state-of-charge distribution throughout the spiral jelly roll, which can be used to determine electric heat losses. The results obtained from this model can then be used to optimize the shape and dimensions of the current collectors as well as the materials used in them.

Table of Contents

Table of Figures

Chapter 1. Introduction

1.1 Background

1.1.1 Lithium ion battery

Batteries have been used since the year 1800 for storing and providing electrical energy. Over time, batteries have evolved, becoming more efficient and compact. This has helped battery technology penetrate all walks of life, from industrial applications to household appliances and cell phones.

Presently, battery research is dominated by an urgency to develop new energy technologies for hybrid electric vehicles (HEVs) and electric vehicles (EVs). The limited supply of energy sources like petroleum and diesel have led to a frantic search for alternative sources of energy to power the next generation of vehicles. Electrical energy offers a promising option for transportation systems in the near future.

Lithium ion batteries have emerged as a popular type of battery for portable electronics, as well as electric vehicles. They are rechargeable, have high energy densities, exhibit no memory effects, and have low self-discharge rates when not in use. However, battery technology for EVs and HEVs has its own challenges including demand for high energy and power densities, high durability as well as safe and reliable operation under heavy usage.

1.1.2 Challenges in battery design for electric vehicles

There are several challenges faced by battery technology for electric vehicles. The

major issues include:

a.) High specific energy (Wh/kg) – The batteries for electric vehicles need to have high energy density to provide sufficient energy in a less weight. Heavier batteries limit vehicle range and acceleration. These batteries need to last longer in a single charge. The long term specific energy target for commercialization is 200 Wh/kg[1] at the cell level. Presently automotive Li-ion batteries have a specific energy of 150 Wh/kg.

b.) Power Density (W/L) – Batteries for electric vehicles also need to have a high power density. There is limited space for batteries in a car. They need to provide sufficient power for the vehicle in the available space. 460W/L[1] is the minimum goals set by United States Advanced Battery Consortium (USABC) for power density in EVs.

c.) Lifetime of a battery – In order to match the current life expectancy of automobiles, batteries for electric vehicles need to have a longer life period. Automobiles have a lifetime of 10-20 years whereas Li-ion batteries for portable electronics last only 2-3 years.

d.) Cost – Currently, the cost of manufacturing and replacing batteries for electric vehicles is very high. They cost as much as $375 - $750/kWh in the Nissan Leaf, $500-$600/kWh for the Volt battery, and $680/kWh for the Tesla roadster[2]. In order to make these batteries appropriate for common use, further research needs to be done to make their manufacturing commercially viable. USABC has a mid-target of $250/kWh and a long term goal of $100/kWh.

[1] Source: USABC Goals for Advanced Batteries for EVs
[2] http://www.fas.org/sgp/crs/misc/R41709.pdf, p 21

e.) Safety – Lithium- ion batteries have serious heating issues. They may rupture and explode at high temperatures. Internal short-circuits in Li-ion battery can cause exothermic reactions leading to thermal runaway. They are safe to be used in small portable devices but scaling them up to 30-40 kWh for vehicles to be used extensively around human life can be risky.

1.1.3 Motivation for modeling EV batteries

It is expensive and time consuming to physically build batteries with different designs and materials to test them for various applications. In order to optimize battery designs and evaluate batteries for electric vehicles, we develop theoretical models and simulate them in software to estimate the performance of these batteries. These models assist us in

a.) Optimizing cell design and battery pack design – The various parameters in the construction of a battery, including the thicknesses of the layers in a cell and the arrangement of the cells in a battery pack can be varied in different simulations. This helps in developing a better cell and battery pack design, tailored specifically for use in electric vehicles.

b.) Performance evaluation – Simulations can be carried out at different currents for different time durations, which help in estimating the energy density and power capability at different temperatures and usage conditions.

c.) Material comparisons – In a Li-ion battery, different materials can be used in the various

parts of the cell. Using these software simulations, the batteries can be simulated with different materials in the various layers and an optimal set of materials for electric vehicles can be determined.

d.) Understanding implication of cell design on aging and safety – Safety and aging are still major concerns for battery designs for EVs. Lithium plating in the anode of these batteries can result in premature aging due to loss of lithium and, in extreme cases, can create internal short circuits in the cell. Uneven charging of the batteries can lead to overcharging in certain regions of the batteries. Exothermic reactions in Li-ion batteries due to overcharging or internal short circuits can lead to thermal runaway causing these batteries to rupture and explode, raising safety concerns and reducing the lifetime of the battery. So Li-ion batteries require special construction and sophisticated monitoring circuits in order to permit their use in mainstream electric vehicles.

The goal of this thesis is to compute the rate of heating and the influence on current distribution in a lithium-ion battery caused by electrical resistances of the current collectors. We do this by supplementing an existing electrochemical model for spirally wound lithium-ion batteries with additional equations that account for the electrical resistance of the current collectors. An electrical network is proposed that accounts for resistance both through the cell sandwich and along the current collectors in a spirally wound battery. A spirally wound jellyroll is treated as an electrical network with discrete node points distributed along the current collectors. In essence, the spiral of the electrochemical cell is modeled as an unwound sandwich of conductive and electrochemically active layers that accounts for the spiral geometry and material properties. Governing equations are developed to solve for voltages at

the node points, current along the current collectors between each pair of node points, and current through the cell sandwich between negative and positive node points.

1.2 *Structure of Lithium ion battery*

The electrochemically active region of a Li-ion battery consists of four parts: the positive porous electrode typically consists of lithium and cobalt metal oxides ($LiCoO_2$); the separator is a fine porous layer of electronically insulating polypropylene and polyethylene film whose pores are filled with Li-conducting electrolyte; the porous negative electrode is typically made of graphite; and the electrolyte which is usually a lithium salt dissolved in organic solvent. The electrochemically active region is sandwiched between the negative current collector, made of aluminum foil, and the positive current collector, made of copper, as shown in Figure 1.

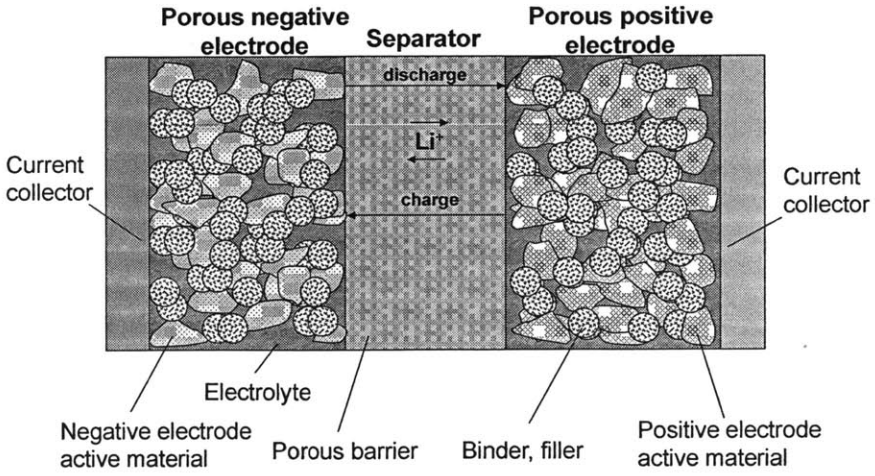

Figure 1 A lithium ion battery consists of the negative electrode, the positive electrode, the separator and the electrolyte. The lithium ions are transferred through the separator from the positive electrode to the negative electrode on cell charge and back to the positive electrode on discharge.

The working principle of a lithium ion battery is the lithium ions going back and forth between the interstitial sites in the electrodes through a process called intercalation. The free energy of Li^+ ion in the negative electrode is higher than the free energy of Li^+ in the positive electrode. During charging, the Li-ions move from the positive porous electrode to the negative electrode lattice. The ions move back to the positive electrode during cell discharge.

This thesis focuses on modeling the current collector resistances of Li-ion battery and studying its effects on the current distribution in spirally wound cell structure. Spirally wound cell sandwich encased in a cylindrical case is the most common format for Li-ion batteries. This is used for laptops and power tools. Li-ion automotive batteries on the other hand are mostly prismatic wound cells. However, in terms of modeling these geometries, cylindrical spirals are the first step towards modeling prismatic cells. They are much more complicated and interesting than stacked cells. Once we have figured out the meshing and modeling in a spiral, the other formats can be built on this model. The cylindrical 18650 cell format is used for modeling in this thesis. To understand this structure, first consider a single "cell sandwich" in a Li-ion battery. This consists of five layers: the negative current collector, negative electrode, separator, positive electrode, and the positive current collector as shown in Figure 2.

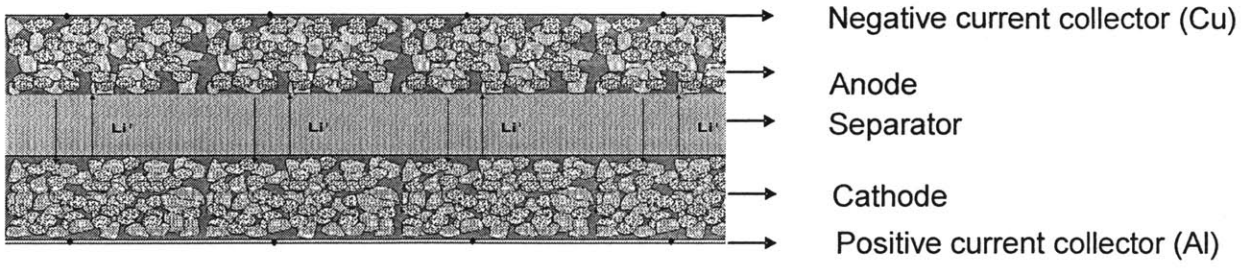

Figure 2 A linear five layer cell sandwich consists of the negative current collector (made of copper), the

negative electrode (anode), a single separator layer, the positive electrode (cathode) and the positive current collector (made of aluminum)

This "single cell sandwich" is then modified to form a "double cell sandwich". In order to understand the double cell sandwich, conceptually imagine a single cell sandwich reflected along the positive current collector to form an eight layer structure consisting of the negative current collector, anode layer, a first separator (separator 1), cathode layer, positive current collector, a second layer of cathode, a second separator (separator 2), and a second layer of anode as shown in Figure 3.

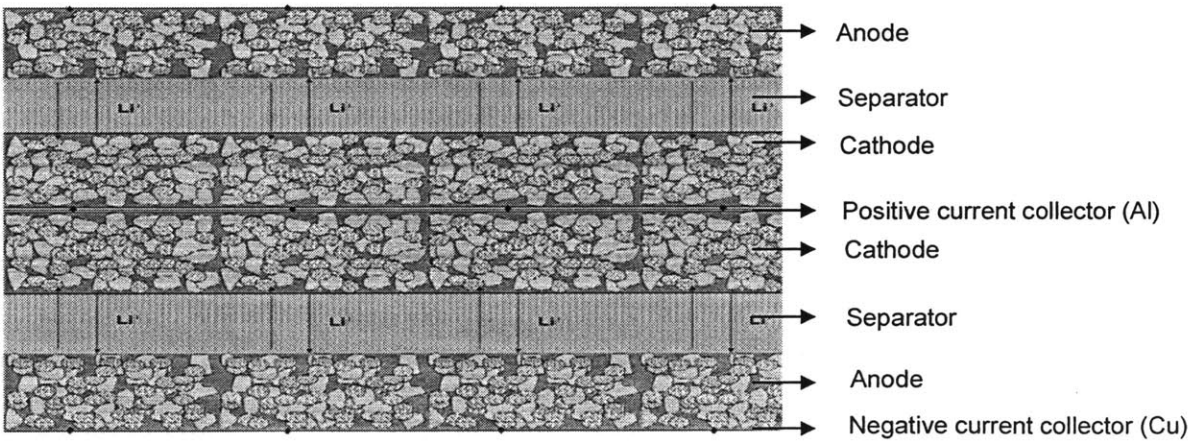

Figure 3 Eight layers of an unwound spiral of a spirally wound lithium ion battery. This has two separator layers. Conceptually it is the single cell sandwich reflected along the positive current collector.

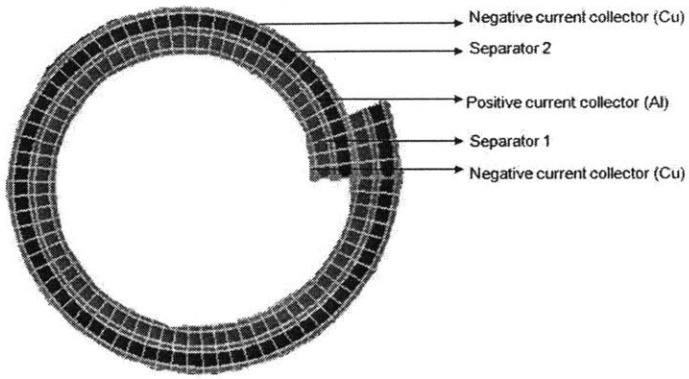

Figure 4 A segment of the spiral cross-section of a spirally wound Li-ion battery showing the current collectors coated with electrodes on both sides. The magenta color represents separator 1 and the blue color represents separator 2.

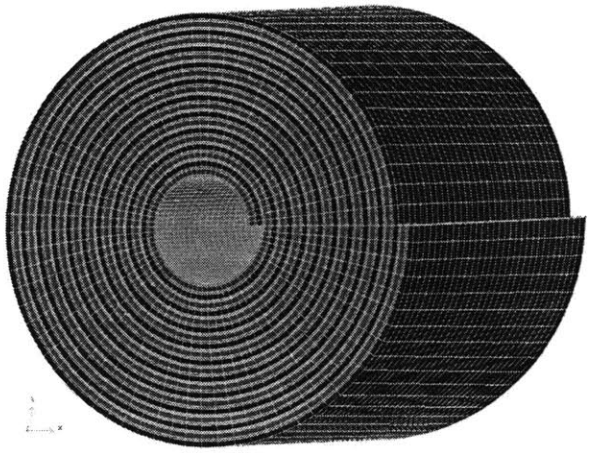

Figure 5 A spirally wound jellyroll typically consists of 20 windings of the eight layer cell sandwich that is shown before in Figure 3.

This eight layer structure shown in Figure 3 is then wrapped into a spiral that makes the spirally wound jellyroll as shown in Figure 4 and 5.

1.3 Electrical Network Model

Most of the research in modeling of lithium ion batteries has focused on the thermal and electrochemical domains of the battery. The cell sandwich structure has been extensively analyzed for the heat distribution due to its electrochemical properties. In this thesis, we model the current collectors of the battery and develop the electrical domain. The electrical resistances of the current collectors affect the current distribution in the cell spiral. This gives a better estimate of the state-of-charge and voltage distributions in the battery with repeated charge and discharge cycles. This also gives insight into the aging and safety issues arising in specific regions of the Li-ion battery.

This modeling helps in accounting for the heat generation in the current collector due to the electrical resistance. This would also help us model temperature dependent resistances for the current collectors and select the ideal materials for the same. This work is outside the scope of the thesis, but can be done in the future to gain more insight into Li-ion battery design and performance using the model developed in this thesis.

With the electrical network modeling the appropriate design parameters for the current collectors can be decided. Thick current collectors reduce the net energy storage capacity (since they reduce the amount of active material in a given volume) whereas thin current collectors tend to increase the thermal losses due to high electrical resistance. Thus, this model can help in establishing optimal geometric parameters for the cell design.

In Chapter 2, we begin by modeling the current collectors in a single cell sandwich of a

lithium ion battery. A simple electrochemical model is used to study the effect the electrical resistance of the current collector on the state-of-charge and voltage distribution. In Chapter 3, we expand this model to the spiral structure of the lithium ion battery and integrate it with the electrochemical domain of the cell. We mesh the jellyroll in the radial and azimuthal directions. In Chapter 4, we discuss the mathematical solutions that we used to solve the system of equations developed in chapter 3 for the 2D electrical model. In Chapter 5 we evaluate the results from this model for both power and energy cells by varying the thickness of the layers and the charge and discharge currents. We also run simulations with different tabbing arrangements to study their effect on the state-of-charge distribution of the battery with aging. Chapter 6 summarizes the work in this thesis and provides future directions.

Chapter 2. Single Layer Electrical Network Model

2.1 Single layer of cell sandwich

To inform our understanding of the electrical network, we first develop a one-dimensional (1D) reduced model for a simple unwound cell sandwich with finite resistances in the current collectors. As discussed in Chapter 1 Figure 1, a single cell sandwich is comprised of the electrochemical layer sandwiched between the positive current collector and the negative current collector. We model this simple cell sandwich by representing the current collectors as a series of resistances and the electrochemical layer as effective non-linear resistances. We validate this representation by comparing our model against our intuitive understanding of the current distribution with just a few current collector elements. We also analytically calculate the current distribution for simple cases such as with no electrical resistance in one or both the current collectors, or symmetrical resistances. This model also helps us realize the importance of accounting for the current collectors in simulations for Li-ion battery designs.

2.2 Electrical Network Model

To develop the equivalent electrical model, we consider the current collector as a series of resistances. Each segment of the electrochemical layer is considered to be a non-linear resistance which is derived from the electrochemistry of the cell. These non-linear resistances

are connected between the two current collectors at the nodes between the series resistances. Thus, the equivalent electrical network for this cell sandwich consists of two layers of resistances in series, one for each of the current collectors, connected by equivalent electrochemical resistances.

A single cell sandwich layer marked with the voltage nodes on the current collectors is shown in Figure 6. The equidistant nodes, where voltage across the cell sandwich is computed, are marked on the current collectors. The voltage nodes on the negative current collectors are $V_{N,k}$ and those on the positive current collectors are $V_{P,k}$. The length of the current collector segment between $V_{N,k}$ and $V_{N,k+1}$ is L_N; the effective resistance is $R_{N,k}$. Similarly, the current collector segment between $V_{P,k}$ and $V_{P,k+1}$ has length L_P and resistance $R_{P,k}$.

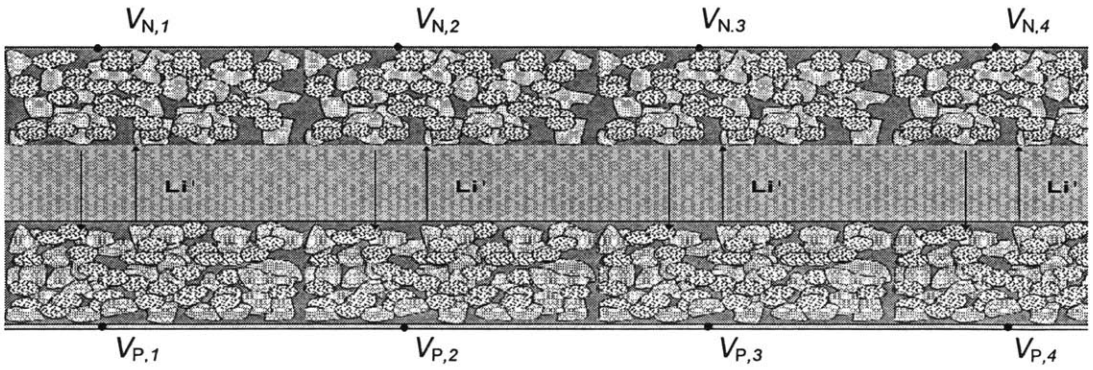

Figure 6 Single cell sandwich with the voltage nodes on the current collectors

The effective electrical network formed is shown in Figure 7. The voltage nodes $V_{N,k}$ and $V_{P,k}$ shown in Figure 7 refer to the same nodes as shown in Figure 6 on the negative

and positive current collectors respectively.

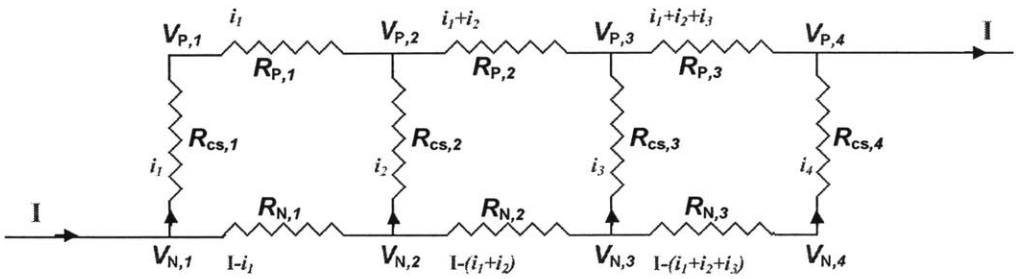

Figure 7 Equivalent circuit for a single layer of the cell sandwich

The cell sandwich is represented as four electrical network elements; each $R_{P,k}$ represents a segment of the positive current collector. Similarly, each $R_{N,k}$ represents a segment of the negative current collector. $R_{cs,k}$ is the impedance of that section of the electrochemically active region of the cell sandwich centered at node k. i_k denotes the current through the k^{th} section of the electrochemical sandwich, also referred to as the k^{th} element. I is the total charge/discharge current that is passed through the cell. The following equations are developed for a cell discharge, when the current flows from the negative electrode to the positive electrode inside the cell.

The non-linear relationship between the voltage difference across the cell sandwich and the current through the cell sandwich is represented by

$$V_{N,k} - V_{P,k} = f_{DF}(\frac{i_k}{A_k}), \qquad (1)$$

where $V_{P,k}$ is the voltage on the positive current collector at element k, $V_{N,k}$ is the voltage

on the negative current collector plate, i_k is the current through the k^{th} element of the cell sandwich, A_k is the cross-sectional area of the k^{th} electric network element through the separator by which the current is scaled. f_{DF} represents the model that describes the relationship between the current and voltage of this region of the cell derived from the electrochemical domain. For modeling the single cell sandwich we use a simplified electrochemical function which is described later in this chapter. For the spiral modeling, we'll use the actual DualFoil (DF) electrochemical model[3] which was developed by the Newman group for modeling Li-ion batteries.

On the negative current collector, current passing through the k^{th} segment is i_k less than the current through the previous element, *i.e.* $I - \sum_{j=1}^{k-1} i_j - i_k$. Thus, by Ohm's law, the relationship between the current and voltage in the negative current collector is given by,

$$V_{N,k} - V_{N,k+1} = (I - \sum_{j=1}^{k} i_j) \frac{\rho_N L_N}{A_N}, \qquad (2)$$

where I is the total current through the battery in amperes, ρ_N is the resistivity of the negative current collector, A_N is the cross-sectional area of the negative current collector and L_N is the length of the negative current collector segment.

Similarly, at the positive current collector, the current through the k^{th} element is i_k more than the current through the previous segment of the positive current collector. So the relationship between the current and voltage is given by,

[3] K.E. Thomas, R.M. Darling, J. Newman, Modeling of lithium batteries, Advances in Lithium-Ion Batteries, Kluwer Academic Publishers, New York, 2002.

$$V_{P,k} - V_{P,k+1} = \sum_{j=1}^{k} i_j \frac{\rho_P L_P}{A_P}, \tag{3}$$

where ρ_P is the resistivity of the positive current collector, A_P is the cross-sectional area of the positive current collector and L_P is the length of the positive current collector segment.

The constraint equation for the total current in the circuit is

$$I = \sum_{j=1}^{M} i_j, \tag{4}$$

where M is the total number of electrical network elements in the cell layer.

The positive voltage of the M^{th} node is used as a reference potential,

$$V_{P,M} = 0, \tag{5}$$

These equations are solved numerically to obtain a current and voltage distribution throughout the cell.

2.3 Electrochemical model

In order to test the electrical network model independently of the actual electrochemical complexity, a simplified electrochemical model has been developed. The function f_{DF} for the voltage difference across the cell sandwich as a function of current through the cell sandwich is given by,

$$f_{DF} = U + IR_{DF}, \tag{6}$$

where U is the open circuit potential of the cell sandwich, I is the current through the cell sandwich and R_{DF} is the electrochemical resistance of the cell sandwich.

The open circuit potential U is given by,

$$U = U_0 + \frac{RT}{F}\ln(\frac{ax}{1-x}), \tag{7}$$

where U_0 is the reference open circuit potential (at $x = \frac{1}{1+a}$), R is the gas constant, T is the temperature, F is Faraday's constant, a is the activity constant, and x is the state of charge of the electrochemical element.

At every time step the change in state of charge (SOC) of the cell is updated. As we are trying to record the SOC at the middle of the timestep, the change from the previous SOC value would be given by $i_{old}\frac{\Delta t}{2} + i_{new}\frac{\Delta t}{2}$, where i_{old} is the current through this region in the previous time step, i_{new} is the current in the electrochemical region in this time step and Δt is the time step size. Thus the state of charge (SOC) of the electrochemical region is updated at each time step using the relation,

$$x_{new} = x_{old} + \frac{(i_{old} + i_{new})}{2}\Delta t \tag{8}$$

where x_{old} is the SOC of this region at the previous time step and $\frac{i_{old} + i_{new}}{2}\Delta t$ is the SOC change at this time step.

2.4 Results and Discussion

The single-cell-sandwich electrical network model has been implemented in MATLAB using the simple electrochemical model discussed in Section 2.3. For these simulations, the reference open circuit potential, U_0 is set at 4V and R_{DF} is set at 1Ω. The cells are simulated at 298K ambient temperature. For these simulations the single cell sandwich is divided into 20 electrical network elements ($M = 20$). 0.1A discharge current is used for the following simulations. In these simulations, discharge current is considered negative ($I < 0$). In all the graphs, the currents are negative, since they are discharging various parts of the cell sandwich. The plotted voltages are measured across the cell sandwich at the voltage nodes. Basic validation of the electrical network model was carried out by implementing simple cases and comparing them with analytical derivations, the results of which are discussed below.

2.4.1 Steady State Analysis

Firstly, the model is analyzed at a steady state without time stepping – both the SOC and hence the open circuit potential of the electrochemical region is a constant. Consider, there is no resistance in the current collectors, which was the assumption prior to the electrical network model. The electrical resistance in both the current collectors is ignored. The voltage and the current distributions are just from the electrochemical zone.

As shown in Figure 8, if we assume that the current collectors have no resistance, the voltage drop across and the current flow through each of the individual electric network elements are the same. There is no voltage gradient in the unwound spiral.

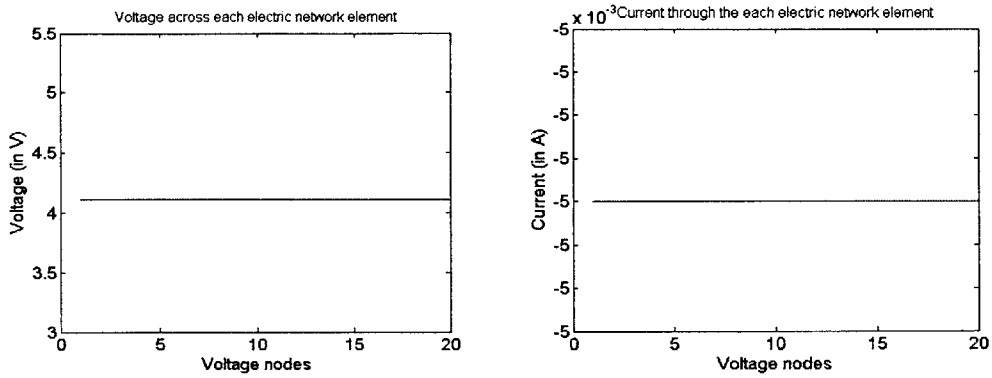

Figure 8 Voltage and current for 20 electrical network elements with zero resistance in current collectors

Now, to verify that the model is physically valid, we assume that both the current collectors have the same resistance, which should give a symmetric voltage and current distribution in the cell.

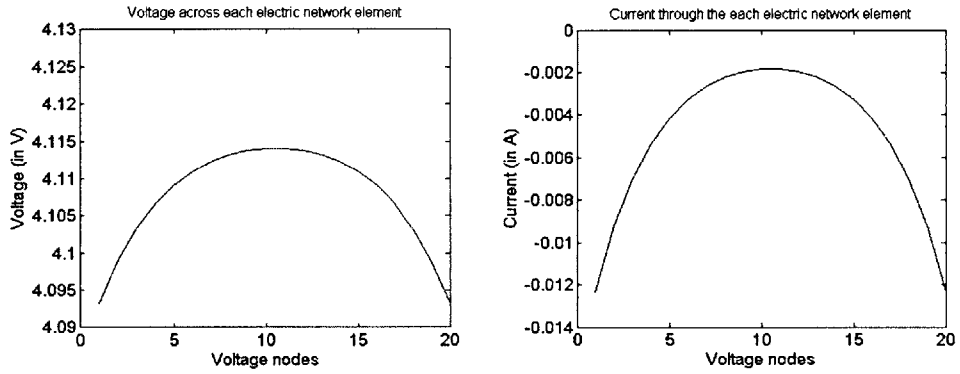

Figure 9 Voltage and current for 20 electrical network elements with symmetric resistance in current collectors

As shown in Figure 9, if the two current collectors have the same resistance, the voltage and the current in the unwound spiral are symmetrical. Since this is a symmetrical resistance network, the maximum current flows in the edges (which are the least resistance path). However, due to the equivalent resistance of the two current collectors, the distribution is symmetrical.

As another validation, we consider one of the current collectors (the negative current collector, in this case) to have no electrical resistance. We would expect a voltage gradient through the spiral. The current flow from the negative current collector to the positive current collector would be maximum at the furthest end in the cell layer.

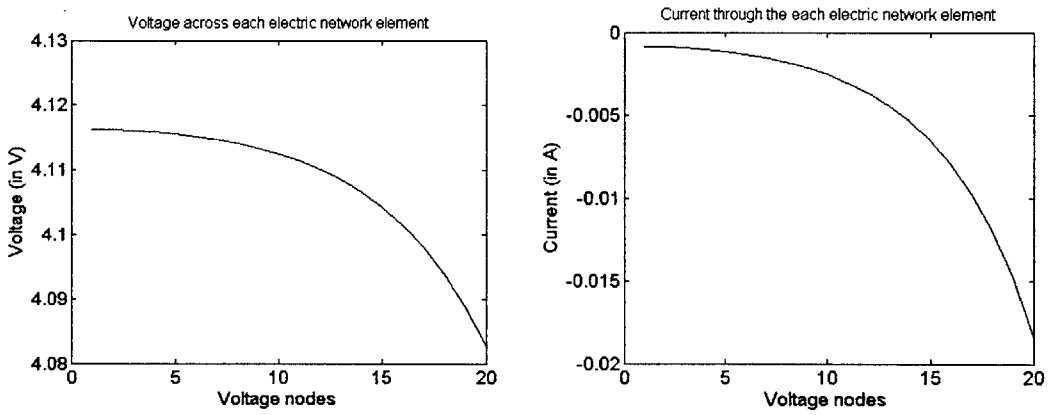

Figure 10 Voltage and current for 20 electrical network elements with asymmetric resistance in current collectors

Thus, as shown in Figure 10 there is a potential drop along the unwound spiral due to the resistance in the positive current collector. The maximum current, flows from one side of the cell sandwich to the other only at the end.

2.4.2 Transient Analysis

In the previous section we only analyzed the network at a steady State of charge and no time stepping. In this section, we allow for time stepping and change of state of charge in the cell. We observe the change in the potential gradients in the cell sandwich as well as the current flow profiles at different part of the cell sandwich at different time steps.

Firstly, we repeat out analysis with no resistance in the current collectors. Over time,

the cell discharges as seen in Figure 11a. But at any given point in time, the voltage throughout the cell is the same as seen in Figure 11b. The current distribution in the cell does not change with time or along the cell sandwich.

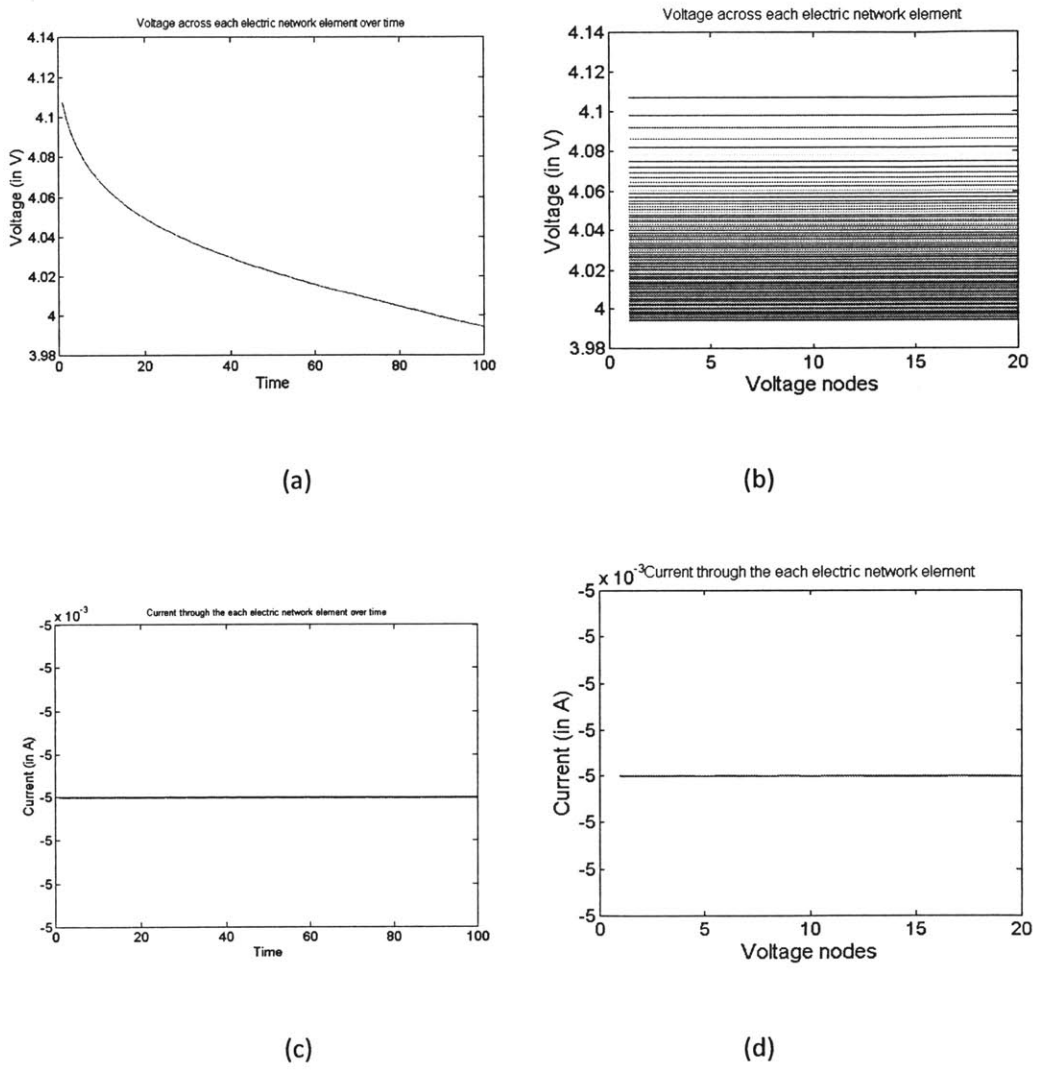

Figure 11 Voltages across and current in each element over 100 time steps. (a) shows the voltage in each of the electrical elements over time. (b) shows the voltage in the electrical elements at each time step. (c) shows the current in each electrical elements over time (d) shows the current at each time step in the electrical elements.

The results seem to be consistent over multiple time steps. Only the cell voltage in each element of the electrical network changes with time.

Lastly, we run a simulation with the standard resistance values in the current collectors. We use aluminum for positive current collector and copper for the negative current collector.

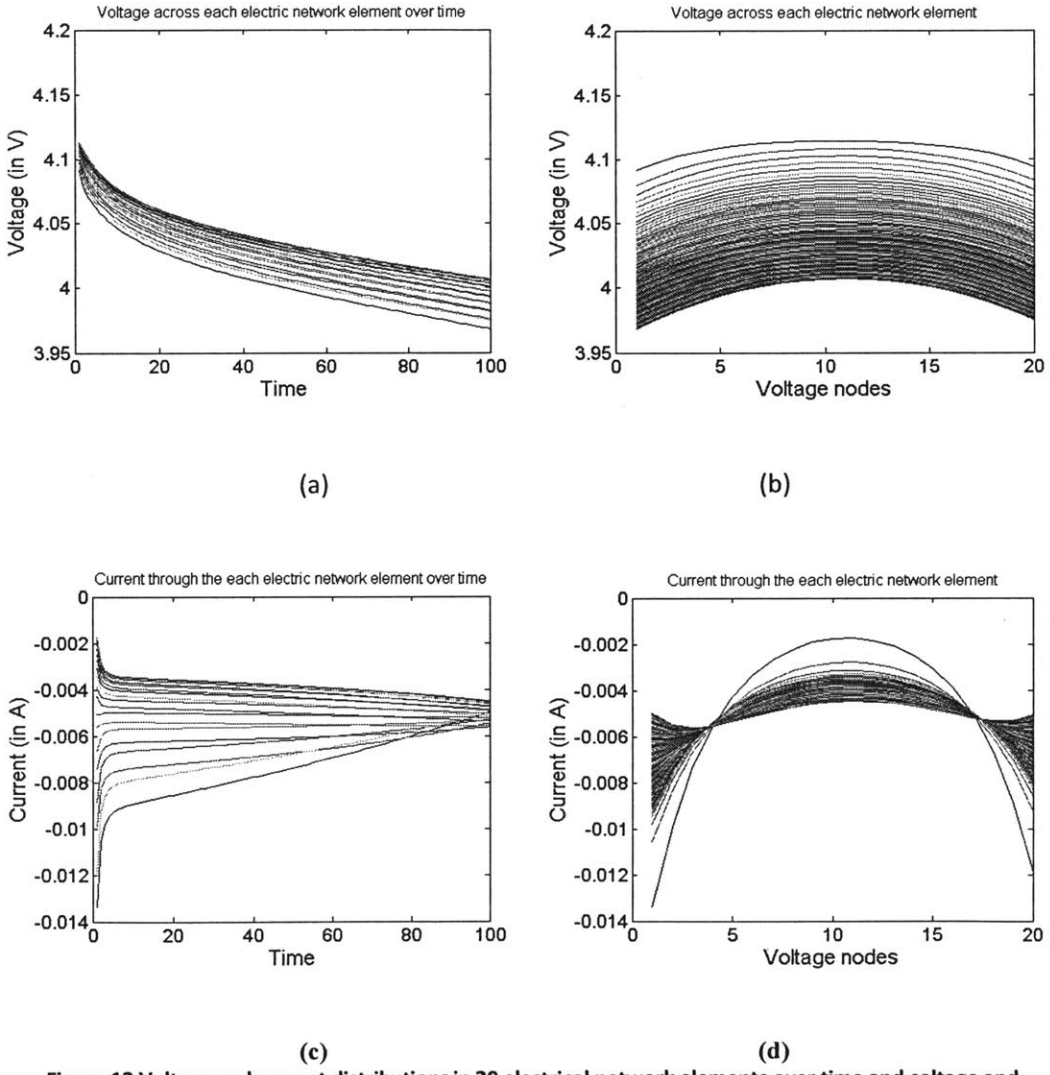

Figure 12 Voltage and current distributions in 20 electrical network elements over time and coltage and current distribution in the cell for each time step.

Figure 12 represents a general case run with 20 electric network elements over 100 time

steps with non-zero resistances for the current collectors. Now as expected, the voltage gradient over time for each element is different. As seen in Figure 12b, the entire cell is discharging with time, but each element has a voltage different from other elements. Similarly the current distribution over time changes for the different elements, based on their location on the cell sandwich. We start noticing interesting results about the current and voltage distributions in the cell sandwich with discharge over time.

With this validation of the 1D electrical network model, we move on to model the spiral cell sandwich which is discussed in the next chapter.

Chapter 3. Electrical Network Model for a 2D spiral

3.1 Spiral Cell Sandwich

In the previous chapter, the battery is considered to be a single cell sandwich extending only in one dimension. However, as shown in Figure 4, the Li-ion battery is an eight-layer spiral with two separator layers. In order to accommodate the spiral structure, the electrical network is modified to have additional electrochemical impedances which model the second cell sandwich. For simplicity, the spiral is meshed at fixed angles as shown by the straight lines in **Figure** 13. After meshing, the nodes on the current collectors where the voltages are computed are selected such that they line up at these angles as in **Figure** 14. This framework makes it possible to reduce the spiral of current collector resistances to a 1D electrical network. The corresponding electrical network circuit model is shown in **Figure** 15. The vertical electrical network elements in the equivalent circuit represent the cell sandwich that includes separator 1 while the slanted electrical network elements represent the cell sandwich that includes separator 2. Based on this equivalent circuit model, a set of governing equations is developed which is solved iteratively to find the current and voltage distributions in the cell.

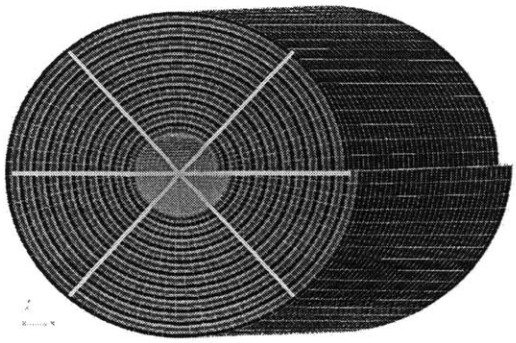

Figure 13 Spirally wound Li-ion cell is meshed in the angular direction. The straight lines on the cross section are mesh lines. $n_\theta = 6$.

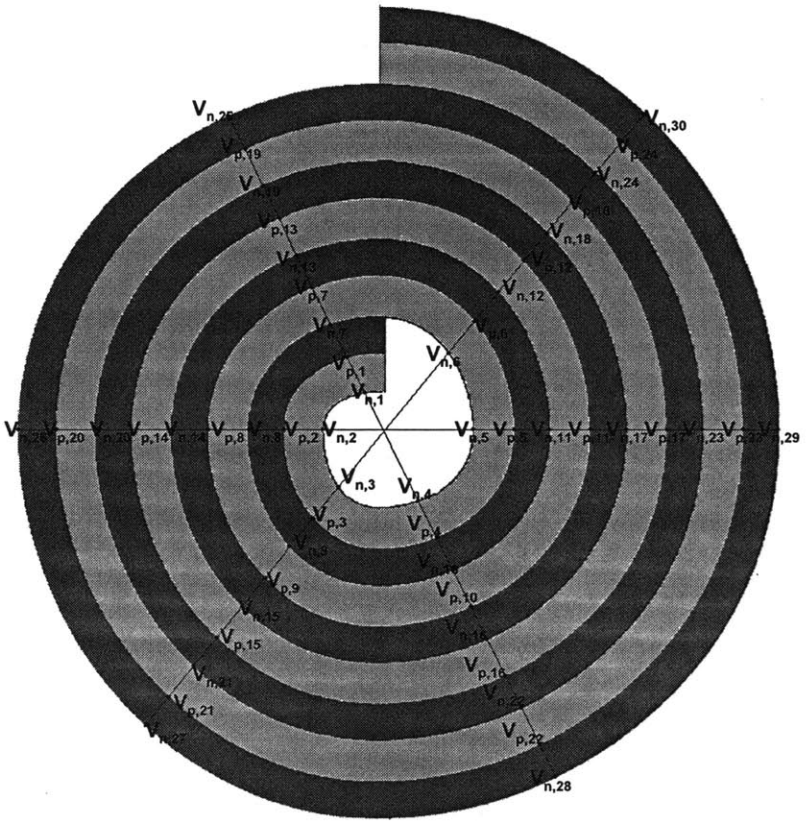

Figure 14 In this spiral, the cyan (lighter shade) represents the elements through separator 1 and the magenta (darker shade) represents the elements through separator 2. Voltage nodes on the spiral are numbered from the inside out in the spiral.

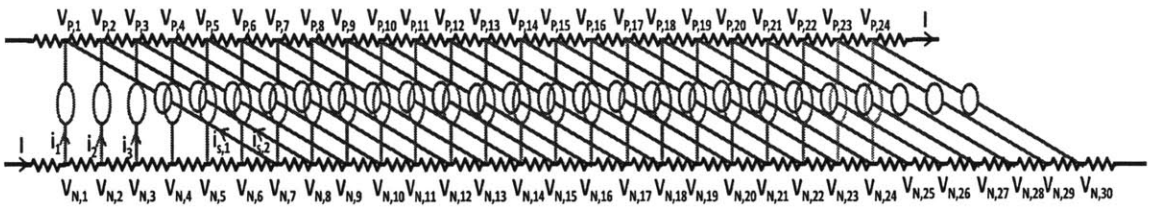

Figure 15 Equivalent circuit representation of the spiral in 1D. The vertical resistor elements represent general electrochemical impedances through separator 1 and the slanted elements represent impedances through separator 2.

3.2 Electrical Network Grid: Setup and Parameters

3.2.1 Setting up electrical grid with spiral meshing

The first step in modeling the electrical network for the spiral is to set up a spiral grid for the cell. This is done under the assumption that the spiral has negative current collectors on both its inner and outer surface. The two restrictions in making the grid are:

a.) Voltage nodes in all the layers should line up along fixed angles.

b.) Each voltage node is located at the center of each electrical network segment.

The electrical network grid is set up from the inside of the spiral. The voltage nodes are numbered from the inside of the spiral to the outside as shown in **Figure** 14. The innermost point on the inner (negative) current collector is considered to be at a zero-radian angle. The first voltage node is placed at an angle of $\frac{2\pi}{2n_\theta}$ radians (where n_θ is the total number of azimuthal divisions) from the innermost point so that it is located at the center of the current collectors in the first electrical network element. The subsequent voltage points are spaced at an interval of $\frac{2\pi}{n_\theta}$ radians along the spiral.

For the other (positive) current collector, the point at a zero-radian angle is at the innermost point of the positive current collector which has a radial coordinate of $r_{\min} + \frac{H^{NCC}}{2} + \frac{H}{2}$ ($r_{\min}$ is the radius of the inner most point of the cell spiral, H is the total thickness of the double layer cell sandwich and H^{NCC} is the thickness of the negative current collector). Just as in the case of the negative voltage nodes, the first positive voltage node is located at a $\frac{2\pi}{2n_\theta}$ radian angle from the innermost point. The subsequent positive voltage points are located at intervals of $\frac{2\pi}{n_\theta}$ radians along the spiral.

3.2.2 Current collector element

The current collector segment between two consecutive voltage nodes in a given current collector is called a "current collector element." Each current collector element in the spiral is represented as a simple resistor in the equivalent resistance network circuit. Like the voltage nodes, these resistors are also numbered from inside out. The current collector segment from the inner most point on the spiral to the first voltage node is the first resistor in the electrical network. The subsequent resistors are numbered accordingly as shown in **Figure** 16.

The number of positive current collector elements and the number of negative current collector elements are calculated by tracing the spiral and calculating the radial position of every voltage node at a $\frac{2\pi}{n_\theta}$ radian angular interval up to the point where this calculated radial position is less than the radius of the spiral. The radial position of each subsequent

voltage node is calculated using,

$$r_{new} = r_{old} + \frac{H}{n_\theta}, \tag{9}$$

where r_{old} is the radial position of the previous voltage node, H is the thickness of the cell sandwich and n_θ is the number of angular divisions of the spiral.

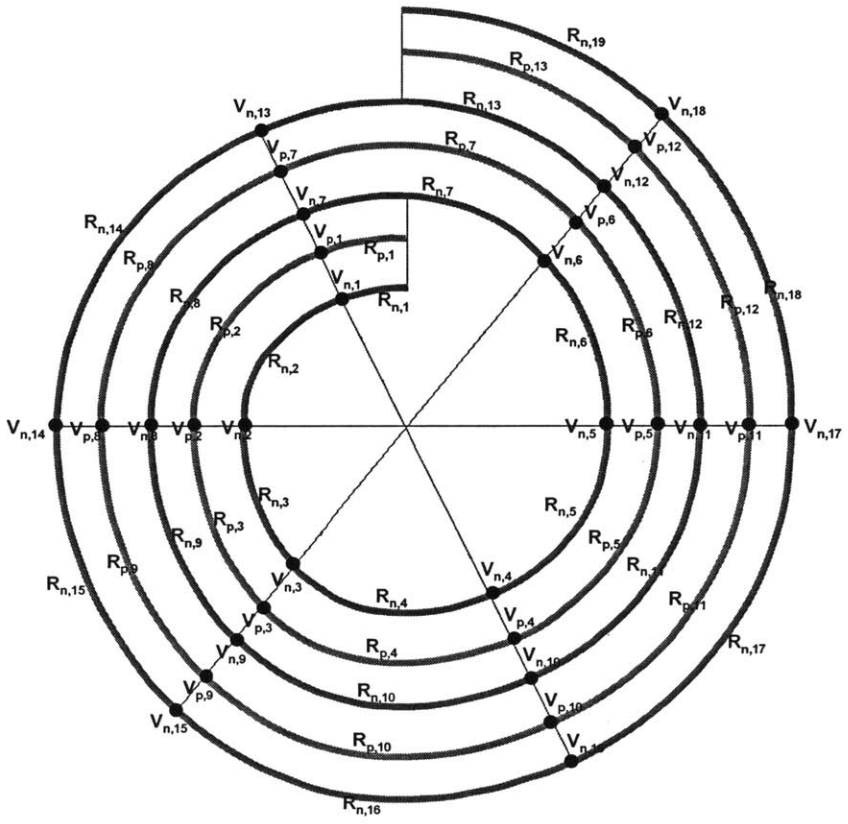

Figure 16 Current collectors with the voltage nodes and resistances marked on them. Green (lighter) represents the negative current collector and the blue (darker) represents the positive current collector. The voltage nodes and the resistances are numbered from the inside of the spiral outward.

The height of the cell sandwich H is given by,

$$H = H^{NCC} + 2H^{NE} + H^{S1} + H^{S2} + 2H^{PE} + H^{PCC}, \qquad (10)$$

where H^{NCC} is the thickness of the negative current collector, H^{NE} is the thickness of the negative electrode, H^{S1} and H^{S2} are the thicknesses of the separator layers, H^{PE} is the thickness of the positive electrode, and H^{PCC} is the thickness of the positive current collector.

The length of each current collector segment is calculated according to the formula for the arc length of an Archimedes spiral:

$$l = \frac{r_1}{2}\sqrt{1+\frac{4\pi^2 r_1^2}{H^2}} + \frac{H}{4\pi}\ln\left(\frac{2\pi r_1}{H} + \sqrt{1+\frac{4\pi^2 r_1^2}{H^2}}\right) - \frac{r_0}{2}\sqrt{1+\frac{4\pi^2 r_0^2}{H^2}} + \frac{H}{4\pi}\ln\left(\frac{2\pi r_0}{H} + \sqrt{1+\frac{4\pi^2 r_0^2}{H^2}}\right) \qquad (11)$$

where r_0 is the radial position of the inner edge of the current collector segment, r_1 is the radial position of the outer edge of the current collector segment and H is the height of the cell sandwich.

3.2.3 Electrical network element

After marking off the voltage nodes and resistances on the spiral grid, the next step is to construct the electrical network elements. Each electrical network element consists of a segment of one cell sandwich with a single separator layer. It contains the two current collectors as its boundaries, with the positive and negative voltage points V_P and V_N at the center of its current collectors. As a consequence of locating the voltage nodes at the midpoint of these elements, the edges of these elements may not align at fixed angles in the

spiral. In **Figure** 17 each color represents an electrical network element. The voltage nodes are aligned on the straight lines shown in the figure.

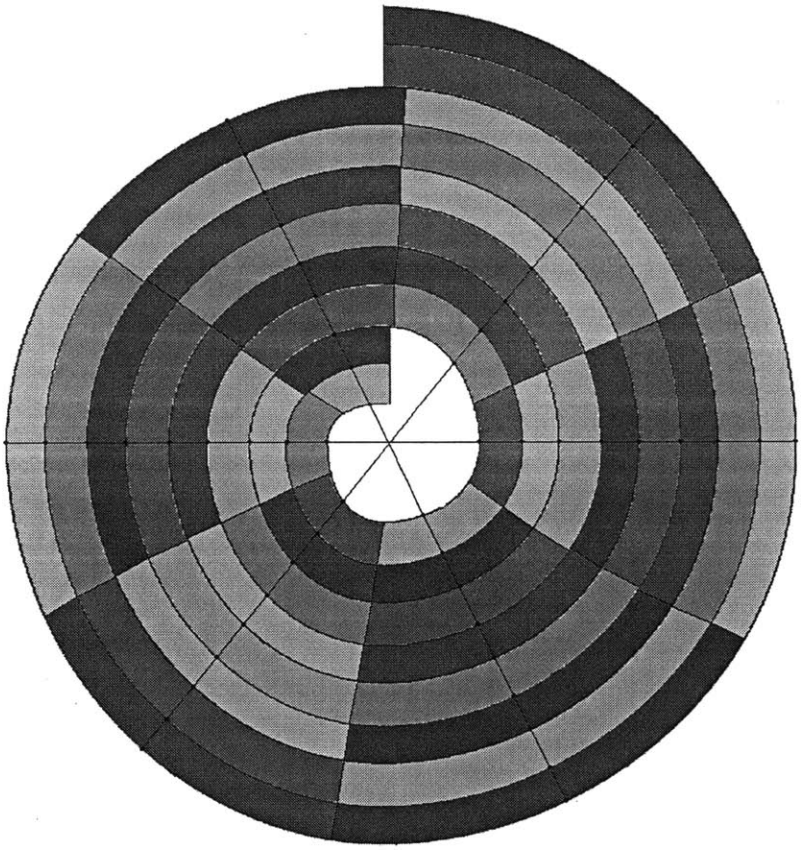

Figure 17 Electric network elements are marked on the spiral. Each color represents one electric network element. The straight lines through the center connect the voltage nodes on the elements. For the equivalent electric resistance circuit the red zones and the blue zones represent the non-linear resistance elements through separator 1 and separator 2 respectively.

For the first electrical network element, the length of its negative current collector (L_N) is twice the length of the negative current collector segment from the innermost point (0 radian angle) to the first negative voltage node. Similarly, the length of the positive current collector (L_P) in the first element is twice the length of the current collector segment from

the inner most point of the positive current collector to the first positive voltage node. The current collector segment lengths of the subsequent electrical network elements are twice the distance from the edge of the previous element to the next voltage node. The current collectors mark the radial boundary of the electrical network element. The ends of these segments define the angular boundary for an element.

The centroid[4] of the electrical network element is the geometric midpoint of that element. $R_{Centroid}$ is defined as the average of the radial positions of the two voltage nodes of the element; $\theta_{Centroid}$ and $Z_{Centroid}$ are the azimuthal and axial positions, respectively, of the voltage nodes. The length of the electrical network element is defined as the average of the lengths of the current collector boundaries as seen in **Figure** 18. L_k^{S1} is the average of $L_{P,k}$ and $L_{N,k}$.

The electrical network elements are numbered from inside out along the spiral; first all the separator 1 elements are numbered, followed by the separator 2 elements.

Typically, the number of electrical network elements in separator 1 and separator 2 are the same. The number of electrical network elements is twice the number of positive current collector elements, assuming that the negative current collector is present both on the inside and outside of the spiral. This should be the case for the spiral with a double cell sandwich.

[4] Usually the centroid is defined as the center of mass of a volume element. But in this case, we use an approximation for the true centroid.

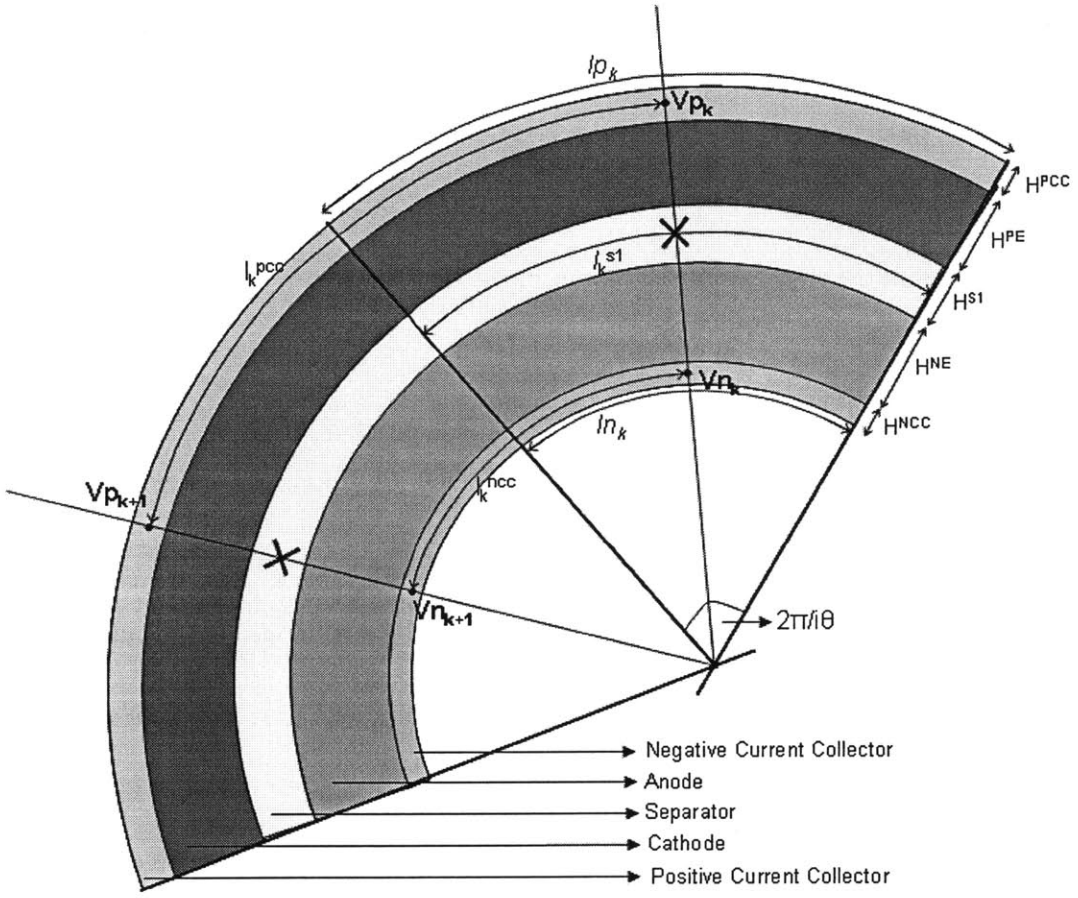

Figure 18 Two electrical network elements. V_n and V_p are the voltage nodes on the electrical network element. L_n and L_p are the boundaries of the element and $L^{s1}{}_k$ is its length. $L^{NCC}{}_k$ and $L^{PCC}{}_k$ are the lengths of the resistors between the voltage nodes. The thicknesses of the various layers are given by H^{PCC}, H^{PE}, H^{S1}, H^{NE} and H^{NCC}. The x marks the centroid of the electrical network elements.

3.3 Mapping between electrical and electrochemical mesh

3.3.1 Electrochemical Grid

In the electrochemical domain, the elements are based on a cylindrical grid. In the cylindrical grid, the meshing is typically done in all three dimensions, radial, angular and

axial. For the purposes of the present electrical network model, we consider only the radial and angular meshing as shown in **Figure** 19. The electrochemical elements are numbered from the inside of the spiral to the outside, starting with the zero-radian angular element.

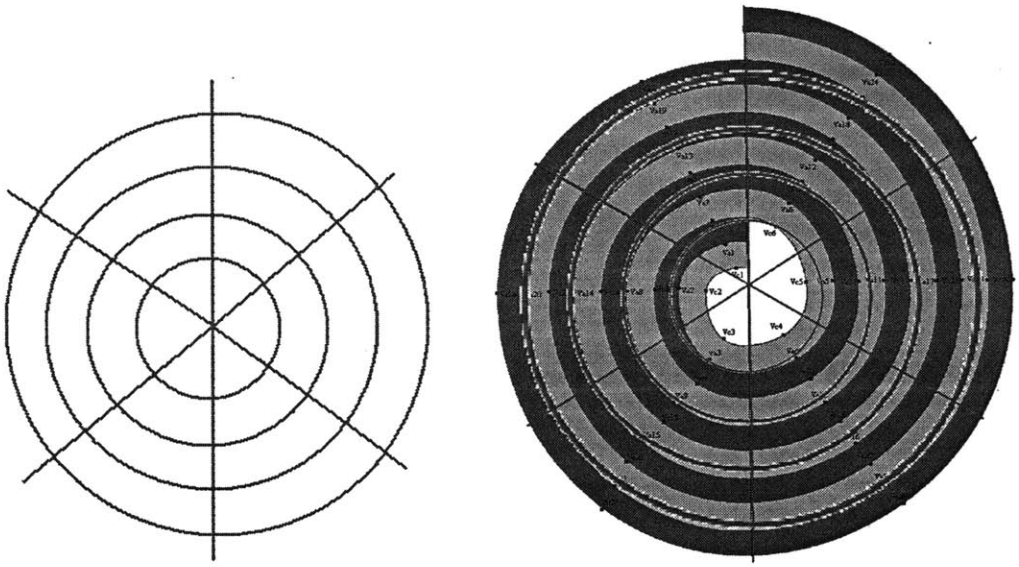

Figure 19 a. Cylindrical Mesh for the electrochemical domain with 4 radial divisions and 6 spiral divisions. b. Cylindrical mesh mapped onto the electrical network's spiral mesh.

3.3.2 Assigning electrical network elements to electrochemical elements

The electrical network elements are assigned to the electrochemical elements so that the voltage and current calculated in the electrical network element can be used in the electrochemical model. The electrochemical model is used to compute a voltage and resistance in each electrochemical element, based on an input current density. These voltages and resistances are supplied to the electrical network model to compute the voltage across each electrical network element via Eq. 12, whereby the local electrical network element's voltage drop is corrected according to the deviation of the element's current density from the

corresponding electrochemical element's current density. The electrical network elements' current densities are in turn averaged to provide the input current density into the electrochemical model for the corresponding electrochemical element. The DF_ID of each electrical network element and each current collector element is updated to the electrochemical element index to which the element belongs. An electrical network element belongs to an electrochemical element if the coordinates of its centroid lie inside that electrochemical element.

3.4 Electric Network equations for the spiral

After the grid is set up and the mapping between the electrical and the electrochemical domain is accomplished, we develop the equivalent electrical network model as shown in **Figure** 15.

The relationship between the potential difference in the voltage nodes on the current collectors and the current through the cell sandwich elements for separator 1 in the roll is represented by Eq. (12)

$$V_{N,k} - V_{P,k} = f_{DF}\left(\frac{i_k}{A_k}\right), \tag{12}$$

where $V_{P,k}$ is the voltage on the positive current collector at element k, $V_{N,k}$ is the voltage on the negative current collector plate, i_k is the current through the k^{th} electrical network element of the cell sandwich in separator 1, A_k is the cross-sectional area of the k^{th} electrical network element through the separator by which the current is scaled, and f_{DF} represents the

electrochemical model that describes the relationship between the current and voltage of the cell layer.

A similar relationship holds for the voltages on the current collectors through separator 2 of the jellyroll,

$$V_{N,k+n_\theta} - V_{P,k} = f_{DF}\left(\frac{i_{s,k}}{A}\right), \tag{13}$$

where $i_{s,k}$ is the current through the slanted element in the electrical network.

The rest of the equations are similar to the equations developed for the 1D electrical network. The relationship between the voltages and currents in the negative current collector for the segments before the slanted elements is given by,

$$V_{N,k} - V_{N,k+1} = \left(I - \sum_{j=1}^{k} i_j\right)\frac{\rho_N L_N}{A_N}, \tag{14}$$

The current-voltage relationship in the rest of the negative current collector segments is given by,

$$V_{N,k} - V_{N,k+1} = \left(I - \sum_{j=1}^{k} i_j - \sum_{l=1}^{k-n_\theta} i_{s,l}\right)\frac{\rho_N L_N}{A_N}, \tag{15}$$

Similarly the relationship in the positive current collector for the segments connected to the slant elements is given by,

$$V_{P,k} - V_{P,k+1} = \left(\sum_{j=1}^{k} i_j + \sum_{l=1}^{k} i_{s,l}\right)\frac{\rho_P L_P}{A_P}, \tag{16}$$

For the rest of the positive current collector segments the relationship is,

$$V_{P,k} - V_{P,k+1} = (\sum_{j=1}^{k} i_j + \sum_{l=1}^{N-n_\theta} i_{s,l}) \frac{\rho_P L_P}{A_P}, \tag{17}$$

The constraint equation on the total current in the network is given by,

$$\sum_{j=1}^{N} i_j + \sum_{l=1}^{N-n_\theta} i_{s,l} = I, \tag{18}$$

The outer most positive voltage is used as the reference potential,

$$V_{P,M} = 0, \tag{19}$$

These equations are solved iteratively to find the current through each element of the model. This current distribution can be used to calculate the heat generation in the cell. In the next chapter we describe in further details how the electrochemical and electrical network models interact and how the numerical solution to the coupled models is obtained.

Chapter 4 Solution methods

4.1 Electrical Network Solution

The set of equations that need to be solved for the electrical network was developed in Chapter 3. The number of equations increases linearly with the number of layers of the spiral or the number of azimuthal divisions in the spiral meshing. To determine the state of the electrochemical values at each time step, a set of non-linear equations need to be solved. This is computationally intensive, both in terms of time and memory space. In order to solve these equations, we use the iterative Newton-Rhapson method at each time step. To optimize the simultaneous solving of the equations, we use the linear algebra package SuperLU.

4.1.1 Interacting with the electrochemical domain to update voltages and currents and obtain Jacobian values

Let K be the set of all the electrical network element indices, i.e., $k \in K$. For each electrochemical element with DF_ID j, the total current (I_{DF}^{j}) is the sum of the currents through each of the electrical network elements, k, that belong to this electrochemical element as described in Chapter 3, i.e., $k \in DF_j$. Similarly, the total area (A_{DF}^{j}) of each electrochemical element is the summation of the separator areas of those electrical network elements. The current density for this electrochemical element is therefore $\hat{i}_j = \frac{I_{DF}^{j}}{A_{DF}^{j}}$. Here, $I_{DF}^{j} = \sum_{k \in DF_j} i_k$ and $A_{DF}^{j} = \sum_{k \in DF_j} A_k$.

For a given current density, the corresponding voltage of the electrochemical element is

$$V_{DF}^{j} = f_{DF}\left(\frac{I_{DF}^{j}}{A_{DF}^{j}}\right), \tag{20}$$

where f_{DF} represents a model for the electrochemical element that takes the instantaneous current density as an input, and along with the complete set of internal states that describes the state of the electrochemical element (i.e., concentration and potential distributions), and provides the instantaneous voltage of the element as output.

Taking a Taylor expansion in the deviation of the electrical network element current density from the respective electrochemical element current density, the potential difference across the cell sandwich for the electrical network element *k*, which belongs to DF element *j*, is obtained as,

$$V_{P,k} - V_{N,k} = V_{DF}^{j} + \left(\frac{dV_{DF}^{j}}{d\hat{i}_{j}}\right)\left(\frac{i_k}{A_k} - \hat{i}_{j}\right) + \mathrm{O}\left[(\Delta i)^2\right], \quad \forall k \in DF_j, \tag{21}$$

where $V_{P,k}$ is the voltage node in the positive current collector for that electrical network element, $V_{N,k}$ is the negative voltage node, i_k is the current through the separator, and A_k is the cross sectional area of the electrical network element.

This coupling between the electrochemical and electrical domain enables the use of two independent meshes for each of these domains. This has a number of computational advantages. In essence a single electrochemical element can be used for the entire jellyroll and still resolve potential and current variations in the jellyroll due to electrical resistance of

the current collectors. With this mapping, the changes can be independently made in each domain without affecting the other one.

4.1.2 Newton-Rhapson method

In order to solve the equations (Eq. (12) – Eq. (19)) for the electrical network, we use the Newton-Rhapson method with the voltage values at the nodes ($V_{N,k}$ and $V_{P,k}, \forall k \in K$) and the currents through each electrical network element ($i_k, \forall k \in K$) as the variables. The Jacobian values for Eq. (14) – Eq. (19) are trivial. For Eq. (12) and Eq. (13), the coefficients for $V_{N,k}$ and $V_{P,k}$ are just 1 and -1. To obtain the coefficients of i_k, for each DF element, three calls are made to the electrochemical domain. The voltages corresponding to the electrochemical current density ($\hat{i}_j$) and $\hat{i}_j$ perturbed by $+\Delta i$ and $-\Delta i$, where Δi is a predefined constant, are calculated as

$$V_{DF1}^j = f_{DF}\left(\frac{I_{DF}^j}{A_{DF}^j}\right)$$

$$V_{DF0}^j = f_{DF}\left(\frac{I_{DF}^j}{A_{DF}^j} - \Delta i\right)$$

$$V_{DF2}^j = f_{DF}\left(\frac{I_{DF}^j}{A_{DF}^j} + \Delta i\right)$$

From these, the first and second order Jacobians are calculated as shown below,

$$J_1^j = \frac{V_{DF2}^j - V_{DF0}^j}{2\Delta i}, \text{ and}$$

$$J_2^j = \frac{V_{DF2}^j - 2V_{DF1}^j + V_{DF0}^j}{\Delta i^2}$$

Thus in the Jacobian matrix, for the equations (1) and (2) for the electrical network element k which belongs to DF_j, the Jacobian elements are

$$b(i_t) = -\frac{J_1^j}{A_t} - \frac{J_2^j}{A_{DF}^j}, t \in DF_j, t = k$$

$$b(i_t) = -\frac{J_2^j}{A_{DF}^j}, t \in DF_j, t \neq k$$

$$b(i_t) = 0, t \notin DF_j,$$

where $b(i_t)$ is the Jacobian coefficient for the current i_t for Eq. (12) and Eq. (13).

After the Jacobian matrix is obtained, it is used to calculate V_P, V_N and i values for that iteration of Newton-Rhapson, which are then used as the guess values for the next iteration.

4.2 Linear algebra solver (SuperLU vs GSL)

The number of equations in the electrical network increases linearly with each round of cell sandwich. Typically in a standard 18650 cell which has 20 rounds in the cell spiral and has 6 azimuthal divisions ($n_\theta = 6$) there would be 486 equations. With a finer electrochemical mesh ($n_\theta = 20$), there would be almost 1600 equations to solve. The large number of equations generates a large jacobian matrix, in each iteration of Newton-Rhapson which poses a challenge to solve them. We first used GSL to solve these equations.

GSL uses matrix inversion to solve the system of equations. Later on, C SuperLU library was used. SuperLU uses LU decomposition and sparse matrix linear algebra routines to solve equations, which was found to be much more efficient as shown in **Figure** 20.

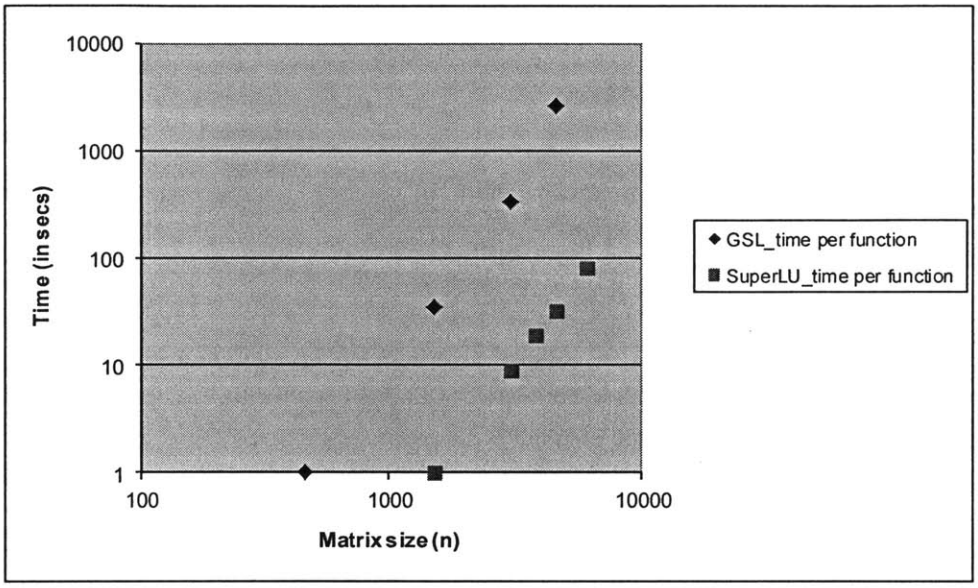

Figure 20 Number of equations vs time take to solve them using GSL (blue) and SuperLU (magenta)

4.3 Iterative solution vs simultaneous solution

The iterative solution method of electrical network is relatively more efficient than the simultaneous solution method used for the prior electrochemical model. A typical simulation is accelerated by a factor of >30.

Assuming that there are n_D electrochemical elements, e_D electrochemical equations for

each element, i_D iterations required to solve each set of these equations, and m_D electrochemical mesh points, the time required to solve the system simultaneously is on the order of $i_D m_D (n_D e_D)^3$, as the $n_D e_D$ equations need to be solved at each step for each of the i_D electrochemical iterations for every m_D mesh point.

With the iterative electrical network, with i_N network iterations, the time taken to solve these equations is $3 i_N i_D m_D n_D (e_D)^3$, because in each electrical network iteration, each electrochemical element is called thrice ($3 i_N$ total calls), and in a given call only the electrochemical equations for that element is solved ($e_D{}^3$).

Using the typical values for each of these numbers (n_D = 20, e_D=10, i_D=4, m_D = 20 and $i_N = 4$) the simultaneous solution is on the order of 6.40E+08 whereas the iterative solution is on the order of 1.92E+07. We see the solution time reduced by a factor of ~30.

The electrochemical model did not need major changes to be integrated with the iterative solution model. The spiral meshing doesn't need to be changed even with multiphysics integration. Computations can be sped up even further using a parallel computing cluster, as the iterative code is parallelizable.

Chapter 5. Analysis for the 2D Electrical network

5.1 Parameters for simulation

In order to evaluate the effects of the electrical network for the lithium ion battery, the cells were simulated under different conditions. Here we describe the parameters that were varied in our sensitivity analysis.

a.) Charge and discharge currents: The rate at which the Li-ion batteries are charged or discharged affects the current distribution as well as the safety and aging rate in a cell. In order to study these effects, the simulations were carried out at different C rates5.

b.) Tabbing arrangements: In a standard cell arrangement, the negative current collector tab is located on the outer side (mantle side) and the positive current collector tab on the inner side (mandrel side) of the jellyroll. Figure 21 shows the mandrel and the mantle sides in a cell spiral. Standard tabbing is the most common arrangement in batteries for mobile applications, such as portable electronics and power tools. We refer to the "mandrel" cell arrangement as one in which both tabs are located on the mandrel side of the spiral; likewise, in the "mantle" cell arrangement both tabs are on the outer side of the spiral. Both "mandrel" and "mantle" arrangements are called "same-side" tabbing arrangements, with the former being more commonly used in cells for portable electronics. The "opposite" tab arrangement is the reverse of the standard arrangement,

[5] A 1C charge rate refers to the current required to deliver the nominal capacity to the cell in one hour (e.g., for a 2.3-Ah battery, 1C = 2.3 A, 2C = 4.6A, and so on).

with the negative tab on the inside and the positive tab on the outside. Figure 22 shows the standard and mandrel tabbing arrangements in an unwound spiral.

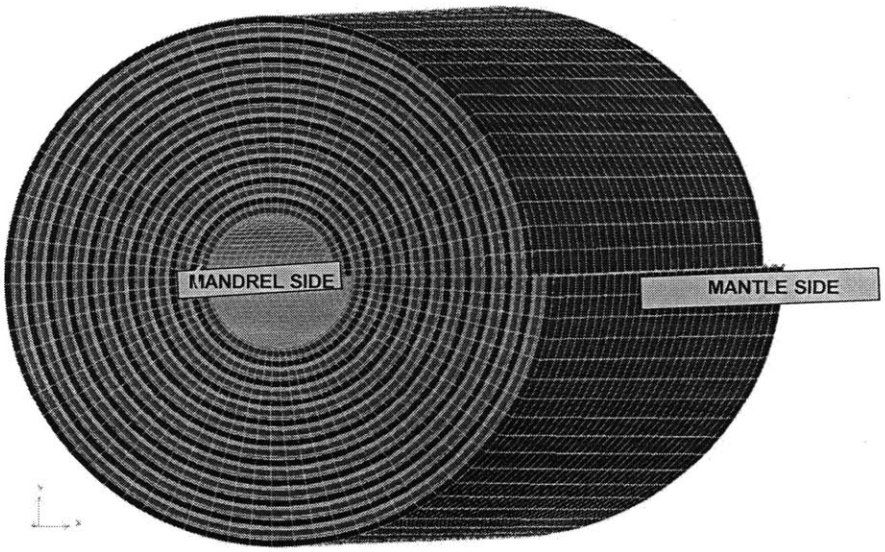

Figure 21 Cell Spiral showing the mantle and mandrel sides. The inside is called mandrel and the outside is the mantle.

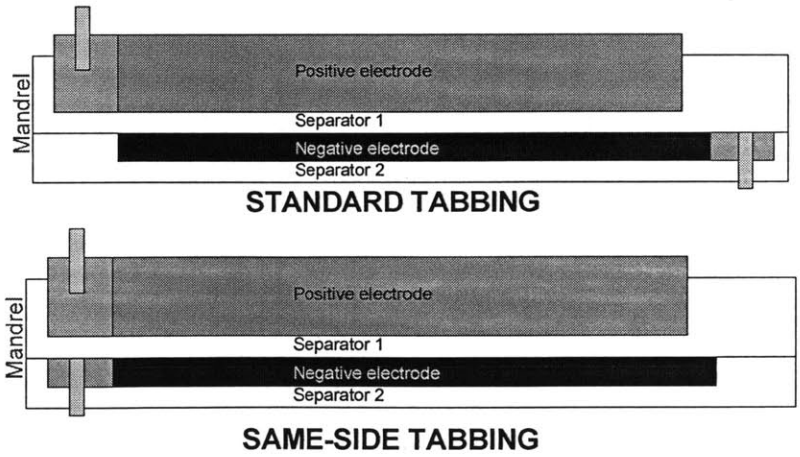

Figure 22 Standard tabbing arrangement and mandrel tabbing arrangement for a Li-ion cell shown in an unwound spiral.

c.) "Energy" and "power" cell designs: The thicknesses of the various layers of the cell sandwich were varied to simulate "power" cells as well as "energy" cells. Power cells, designed for applications with high power-to-energy ratios, such as power tools, have lower capacity, thinner electrodes, and thicker current collectors, whereas energy cells (e.g., for laptop applications) have greater capacity, thicker electrodes, and thinner current collectors. For a given cell volume, the power cells have a longer but thinner unwound jellyroll as compared to an energy cell, as shown in Figure 23.

18650 cell type	Energy	Power
Nominal capacity (Ah)	2.3	1.5
Anode		
Thickness (um)	110	55
CC thickness (um)	4	10
Porosity	0.24	0.39
Cathode		
Thickness (um)	90	45
CC thickness (um)	7.5	15
Porosity	0.15	0.3
Separator thickness (um)	20	20
Spiral length (m)	0.42	0.69

Table 1 Parameters used for simulating the performance of an energy cell and a power cell.

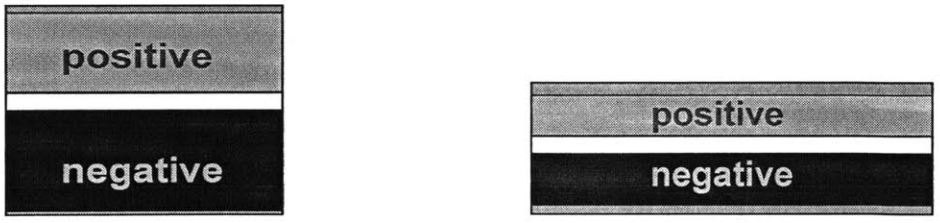

(a) Energy cell (b) Power cell

Figure 23 Energy cell vs power cell design for lithium ion battery. The blue layer represents the positive current collector, the gray is the positive electrode, white represents the separator layer, black is the negative electrode and yellow represents the negative current collector.

d.) Some electrolyte properties were also varied to further analyze the impact of current collector resistance. An "ultra power cell" was simulated, which had the same cell sandwich thickness as the power cell but had superior electrolyte properties (Diffusion coefficient (D) and electrical conductivity (κ) were increased by 3). Furthermore, the particle size in the electrodes was reduced by 100.

The output parameters observed to study the effects of electrical network on cell design are:

a.) Voltage distribution and cell voltage – The voltage distribution in the cell spiral is uniform without the electrical resistance of the current collectors. However taking into account this resistance gives us interesting results about the voltage gradients in the Li-ion battery. The more non-uniform the current/voltage distribution is, the more the cell voltage will deviate from the equilibrium voltage at any given time. We observe the cell voltage under different charge and discharge conditions.

b.) SOC distribution – In an ideal cell with zero current-collector resistance, the state-of-charge is uniform throughout the jellyroll. By introducing the electrical network resistance, different parts of the jellyroll are charged and discharged at different rates. This variation in SOC can cause parts of cell to be overcharged, resulting in premature aging.

c.) SEI thickness – Solid electrolyte interphase (SEI) is the passivating layer that develops between an electrode (negative) and the electrolyte because of the reductive

decompositions of a small amounts of organic electrolytes6. The model used for the SEI thickness growth is described in detail by Christensen and Newman7. With aging, the SEI grows thicker on the electrode particles. Cyclable Li is consumed in forming SEI which leads to irreversible capacity loss in a cell. Also, a thicker SEI is more resistive, leading to higher impedance in the electrochemical domain. So studying the variations in SEI thickness help us understand aging of the cell. A non-uniform SEI thickness in the cell spiral indicates that different parts of the cell age differently. This differential aging can compromise the safety of using the battery earlier than would uniform aging.

d.) Overpotential – Surface overpotential in a cell is defined as the potential of the working electrode relative to a reference electrode. The observed cell voltage above the expected equilibrium cell voltage is called the cell overpotential (or spiral overpotential, in this case). Observing these overpotentials show the effect of electrical network resistance on the operational cell voltage.

The various input parameters used in the electrical network modeling for baseline simulations are shown below in Table 2.

Table 2 Parameters used in the electrical network modeling

Parameter	Default value
Number of axial meshpoints in electrochemical domain (N_Z)	1
Number of radial meshpoints in electrochemical domain (N_R)	8
Number of azimuthal meshpoints in electrochemical domain (N_θ)	3
Minimum SOC of the cell	0.026434

[6] Lithium-Ion Batteries: Solid-Electrolyte Interphase by Perla B. Balbuena, Yixuan Wang
[7] J. Christensen and, J. Newman, *J Electrochem. SOC.*, **151 (11)**, A1977 (2004).

Maximum SOC of the cell	0.99
Minimum voltage of the cell (V_{min})	2.8V
Maximum voltage of the cell (V_{max})	5.17V
Ambient temperature for isothermal simulations (T)	298K
Number of azimuthal divisions for the electrical meshing (n_θ)	6
Inner radius of the spiral (r_{min})	0.001715m
Outer radius of the spiral (r_{max})	0.008295m
Height of cell spiral	0.057m
Resistivity of negative current collector	1.68e-8 Ω-m
Resistivity of negative current collector	2.82e-8 Ω-m

5.2 Current collectors affect cell potential and SOC distribution

Discharge of a "standard" cell was simulated at different currents, first without taking the current collector resistances into account and then with the electrical network resistances included. As seen in Figure 24, the discharge paths for cells with and without current collector impedances are different. The difference in cell voltage between the two paths was found to be proportional to the discharge current as seen in Figure 25. This proportionality, or apparently "ohmic" behavior, implies that we should be able to calculate the impedance for a given set of jellyroll and cell sandwich dimensions and correct the voltage curves by the product of the impedance and the current. However as seen in Figure 26, during a cell discharge different parts of the jellyroll have different states of charge. This is due to the current collector impedance affecting the SOC distribution through the spiral. This variation in SOC distribution can cause faster cell aging than expected when considering a simple ohmic correction.

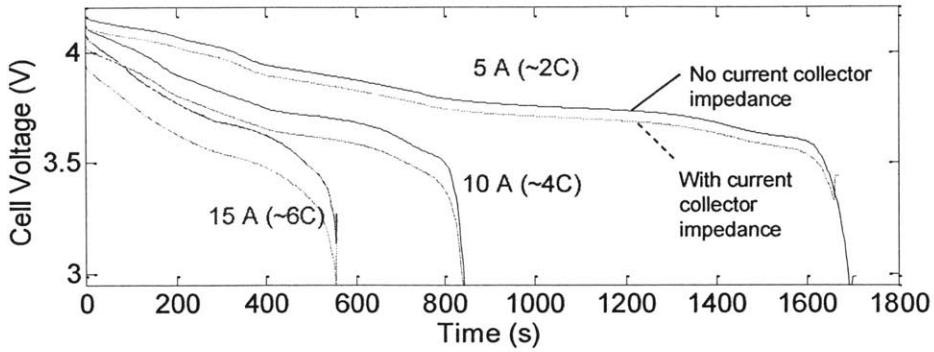

Figure 24 Cell discharge at different currents. The current collector impedance affects the cell voltage, with a correction that is proportional to the current.

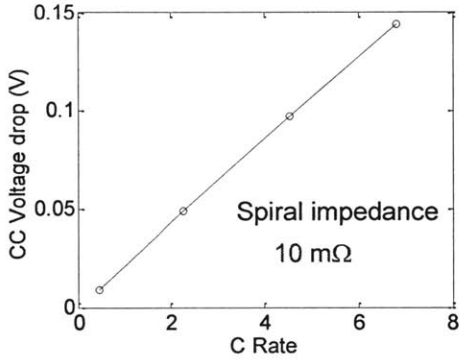

Figure 25 Impedance due to the current collectors have an ohmic behavior, i.e., the difference in cell voltages (see Figure 3) is proportional to the discharge current. The "spiral impedance" of a standard cell was found to be 10 mΩ.

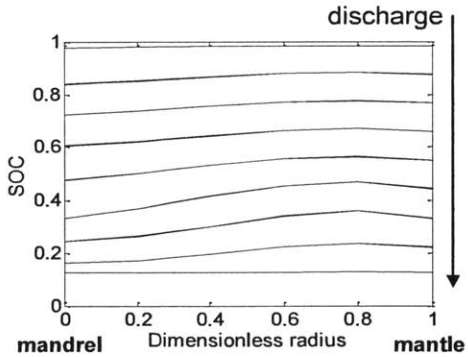

Figure 26 Variation of the state of charge (SOC) of the cell during discharge. Different colors represent evenly spaced time step during the cell discharge.

5.3 *Effect of tabbing arrangement*

5.3.1 Tabbing influences cell over-potential, SOC distribution, and SEI thickness

As discussed before, tabbing is a choice made in cell design. The simulations were run with the same discharge current for different types of tabbing. As seen in Figure 27, the difference between cell voltages due to current collector impedances doubles with same-side tabbing (mandrel) as compared to standard tabbing.

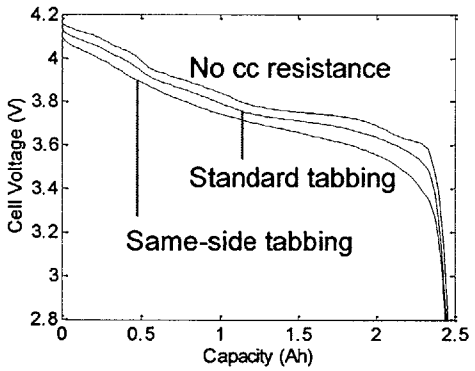

Figure 27 Influence of tabbing on cell voltage during discharge. For this cell design, same-side tabbing has nearly 2x more overpotential than standard tabbing.

Tabbing arrangements also affect the SOC distribution in a cell as seen in Figure 28. The variations of SOC seen through the cell spiral in case of same side tabbing can be significantly higher as compared to the SOC variations with standard tabbing arrangements, although the magnitude of the difference depends strongly on the cell design and material properties.

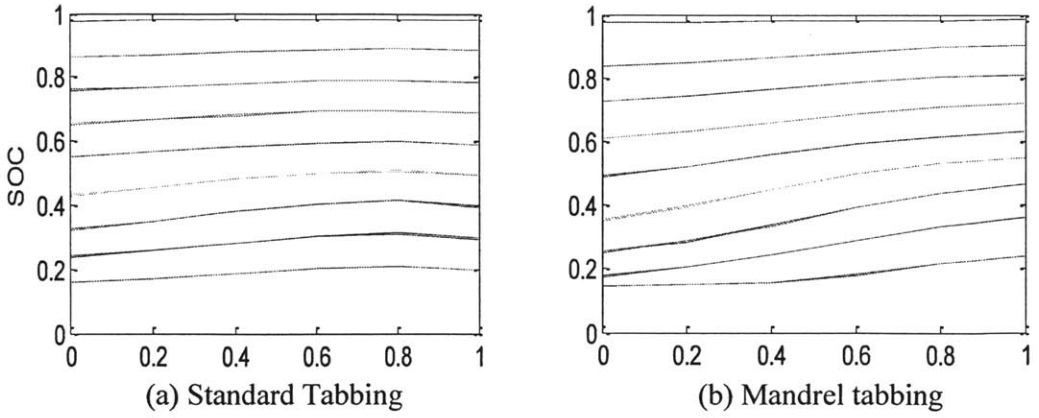

Figure 28 SOC variations during cell discharge at different time steps with tabbing. Subplot (a) shows the SOC distribution during discharge with standard tabbing. Subplot (b) shows the SOC distribution with mandrel tabbing.

The SEI thickness is also affected by the tabbing arrangements due to the effects of electrical network. At the end of complete discharge, the average SEI thickness profile along the cell spiral is more non-uniform for same-side tabbing as compared to the standard tabbing arrangement. However, the average SEI thickness is almost identical for the two cases.

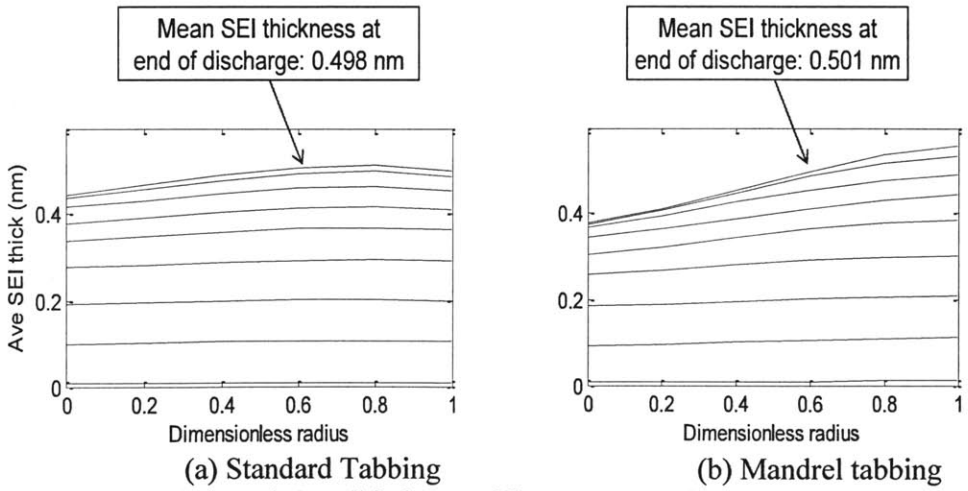

Figure 29 SEI thickness during cell discharge at different timesteps. The SEI thickness is more non-uniform in case of mandrel tabbing (b) vs standard tabbing (a). Mean SEI thickness at the end of discharge is slightly higher for same-side tabbing.

The effects of tabbing on the non-uniformity of the SOC and average SEI thickness distribution are also seen during the charging of the battery. As shown in Figure 30, at the end of charging, Mandrel tabbing showed 7% variation in SOC distribution while the standard tabbing shows only 2% variation. Similarly as seen in Figure 31, the average SEI thickness at the end of charge varies 11% for a standard tabbing as compared to 27% for mandrel tabbing.

This implies that standard tabbing is preferable for a lithium ion cell design, as it seems to be safer since it ages more uniformly throughout the cell spiral. Non-uniform SOC and voltage distributions cause different parts of the cell to be overcharged and hence unsafe for use.

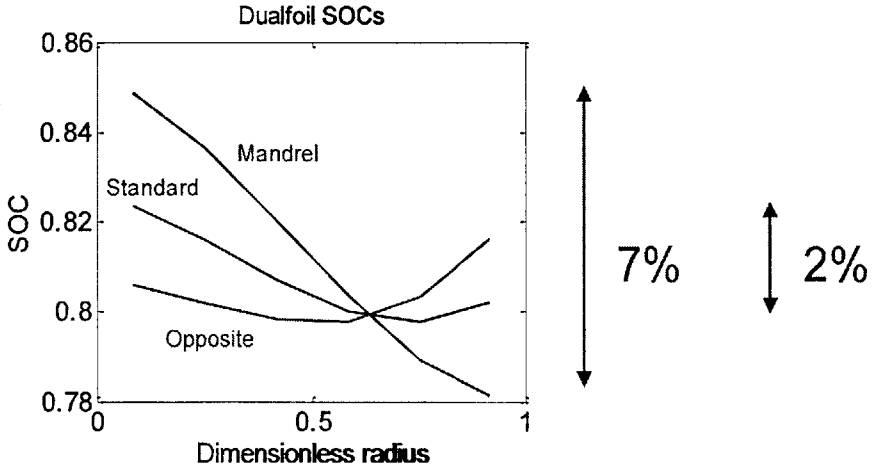

Figure 30 End of charge SOC distribution for a power cell at 10A. Same-side tabbing has a 7% difference through the spiral whereas the standard tabbing only shows a 2% variation.

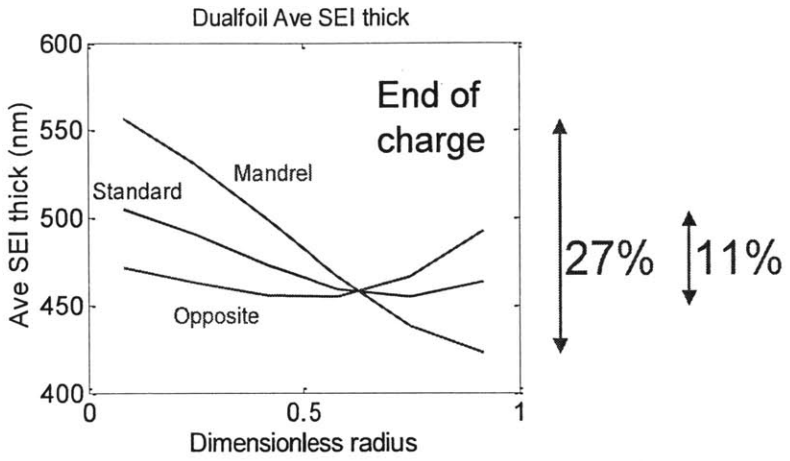

Figure 31 Average SEI thickness variation at the end of charge in a power cell charged at 10A. Same side tabbing shows a 27% variation whereas standard tabbing shows only 11% variation.

5.4 Energy vs power cell

Several simulations were run with energy and power cells. They were charged at various C rates and the spiral overpotentials caused due to the electrical network in both cases were observed. These plots are shown in Figure 32. The dashed lines represent the cell voltage profile while charging without including the resistance from the current collectors, whereas the solid lines represent the profiles with the resistances included.

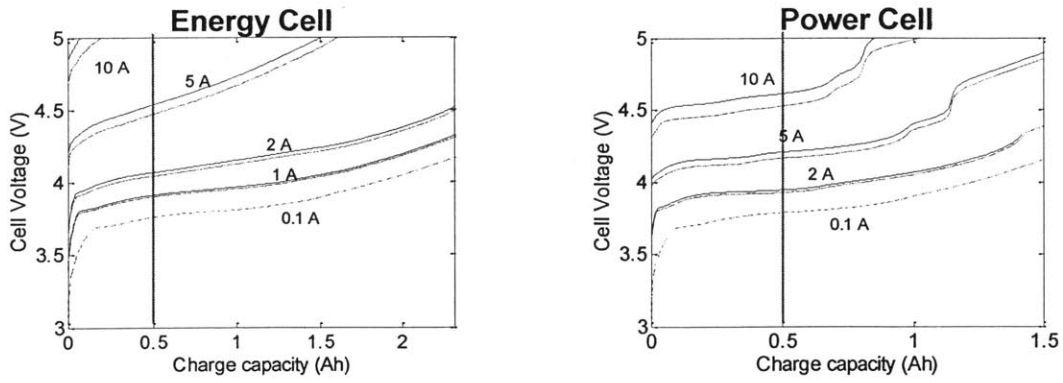

Figure 32 Cell votage vs cell capacity plots for both energy and power cells at differenct C rates.

As observed from these plots, there seems to be an ohmic dependence of the increase in cell overpotential upon the applied current, with the linear resistance depending upon the cell design. To illustrate this, the cell overpotentials at different charging rates were computed after 0.5Ah of charge were passed. These overpotentials were aligned as shown in Figure 33, thus illustrating the apparently ohmic spiral impedance. However, as noted earlier, simply adding an ohmic term to the cell overpotential does not capture the nonuniformity in SOC distribution imparted by the current collector resistance.

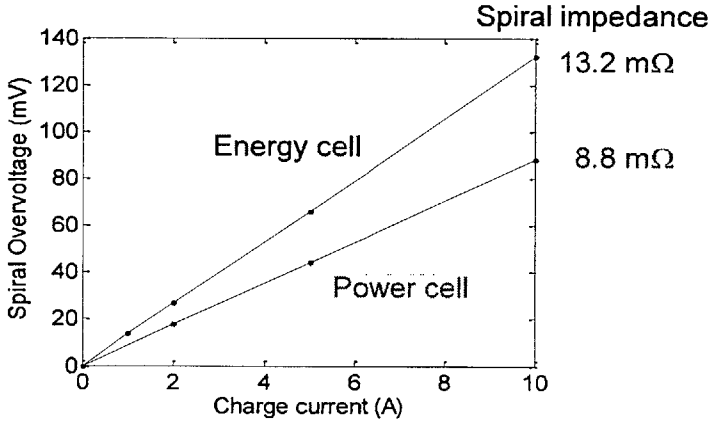

Figure 33 Ohmic spiral impedance of an energy cell compared to a power cell

The electrochemical resistance in the cell sandwich was then reduced to simulate an ultra-power cell. The spiral impedance from the ultra power cell is still ohmic (linear) but instead of it reducing further with respect to power cells, it actually increases. This shows the electrochemical resistance seems to have an opposite effect as compared to the current collector resistances

Decreasing the cell-sandwich (electrochemical) resistance leads to a more nonuniform current distribution because the influence of the current collectors is relatively higher. A more nonuniform current distribution means higher local current density in some parts of the jellyroll (i.e., near the tabs). The electrochemical impedance is nonlinear with respect to current density (i.e., mass transfer overpotentials increase exponentially with current density), which cause these "high current density" regions. This "impedance boost" associated with this have an impedance that is greater than that which would correspond to the average current density. Thus the current nonuniformity gets incorporated into the "spiral impedance" that we calculate by taking the difference in cell voltage for the two models. This can be shown mathematically, but that is beyond the scope of this thesis.

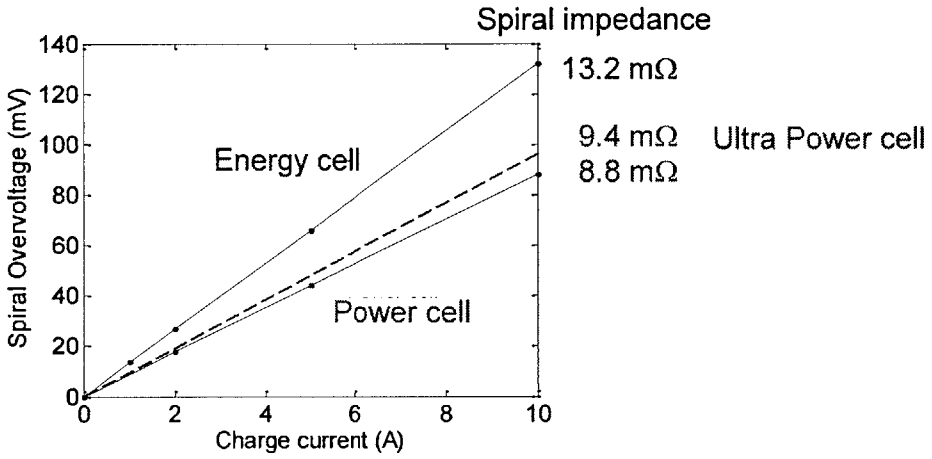

Figure 34 Spiral impedance for an ultra power cell as compared to a power cell or an energy cell

5.5 Lithium plating

During cell charging, if the current is too high, the transport rate of Li^+ ions is greater than the rate at which they can be intercalated into graphite at the negative electrode. This

leads to the deposition of Li^+ ions as lithium metal on the graphite surface. Lithium plating is thermodynamically favorable when the surface overpotential, $\Phi_{Solid} - \Phi_{electrolyte}$, is less than 0, i.e., the potential inside the graphite is less than the potential in the electrolyte medium just adjacent to the graphite. This metal deposition can lead to capacity loss (i.e., loss of cyclable Li) as well as short circuits and other safety issues.

In an energy cell, with a 5-A charging current, a 10 mV spread was observed in the surface overpotential as shown in Figure 35. Thus, the current collector resistances cause a variance in Li plating driving force in the cell spiral.

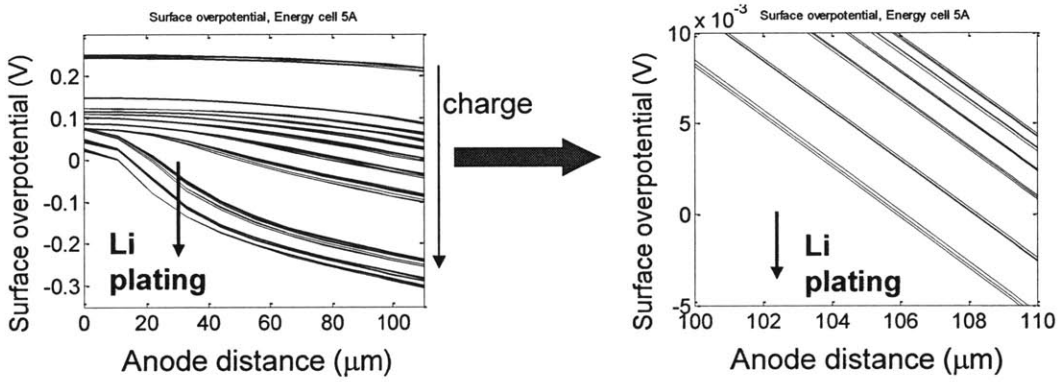

Figure 35 Lithium plating is observed in an energy cell with 5A charging current. Each band contains profiles for all electrochemical elements at fixed time intervals.

In an ultra power cell, with high charging currents (10A), tabbing influences the variation in the lithium plating driving force as shown in Figure 36.

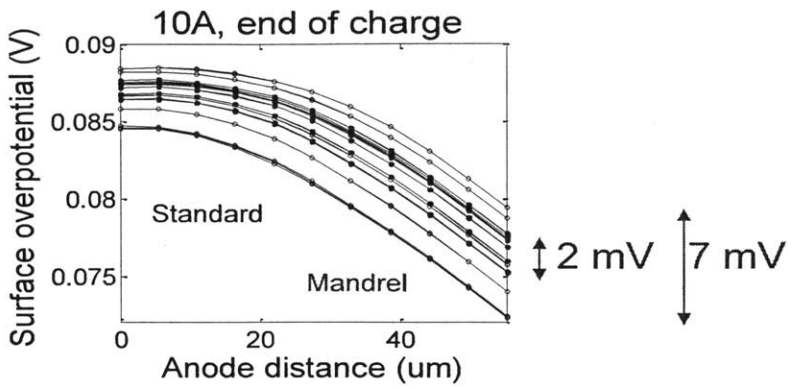

Figure 36 Tabbing influences driving force for lithium plating. Standard tabbing shows only 2 mV variation whereas Mandrel tabbing shows 7 mV variations.

These examples illustrate that the electrical network gives us insight into the safety and aging of lithium ion battery with different designs. Material properties and their influence can also be studied using this model. Simulations of cells with different materials inform us about the tradeoffs between different tabbing arrangements and cell designs (e.g., power vs. energy cells). By optimizing the cell design to maximize performance for a particular application (e.g., one with an average discharge rate of 1C and charge rate of 2C), one can evaluate the benefit of one material or materials set over another.

Chapter 6 Future work and Conclusion

6.1 3D extension

So far the electrical model has been developed and analyzed for a 2D model. This doesn't account for any voltage gradient in the axial directions. In order to account for the current flowing in the current collectors along the vertical direction, the spiral needs to be meshed in the axial direction as well, as shown in Figure 37.

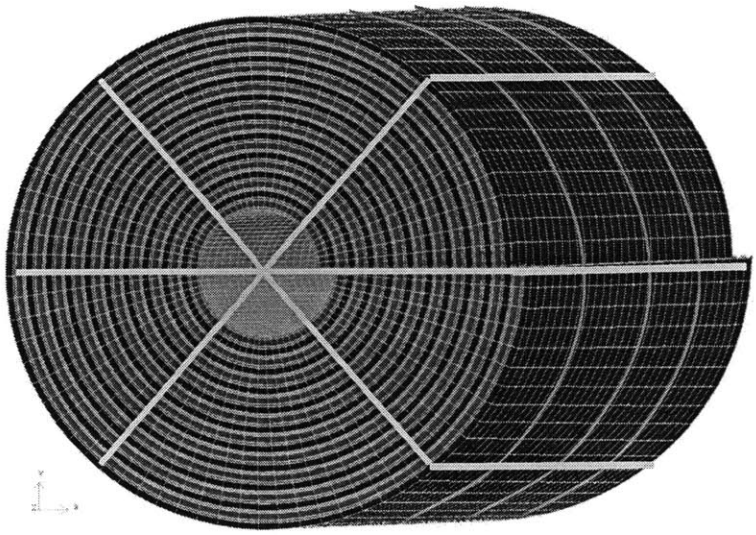

Figure 37 3D Meshing of the spiral with 6 azimuthal sections and 4 vertical sections

Each of these axial elements can be reduced to the 2D model that has been developed so far, connected to each other with vertical current collector resistors. As seen in Figure 38, the equivalent electrical network model has a 3D network of current collector resistance, each current collector sheet has a 2D grid of resistance. The sheets of 2D resistances of the positive and negative current collectors are then connected at their voltage nodes by non-

linear electrochemical resistance as before, based on the spiral geometry of the cell.

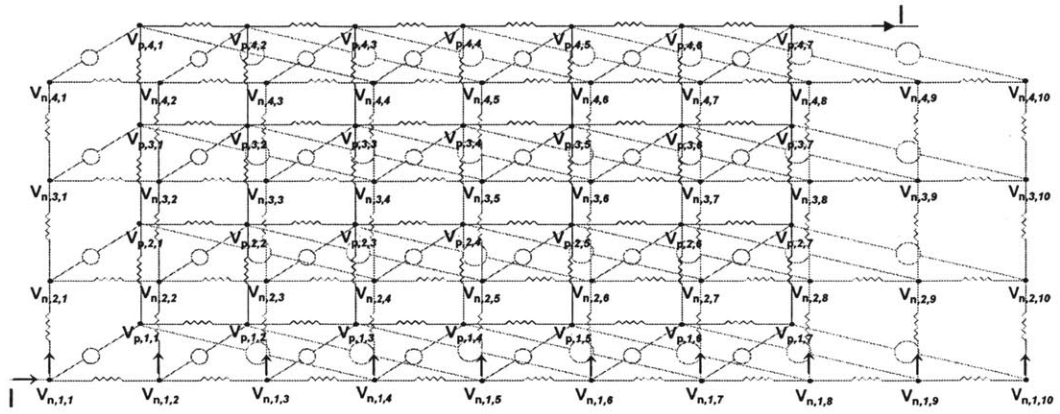

Figure 38 Equivalent electrical network circuit for 3D modeling

The set of equations can be developed just as they were for the 2D model which on solving would give us the current and voltage distributions. This model can also be used to optimize tabbing arrangements in a cell and the connection lengths between the tabs and the current collectors.

6.2 Integration with the thermal model

The electrical network model can be integrated with the thermal model to account for the heat generated in cell due to the ohmic resistance of the current collectors. The mapping between the thermal and the electrical domain can be done through the electrochemical domain. The heat generated in the electrical domain of the electrical network elements can be uniformly distributed throughout the volume of the electrochemical element to which these electrical network elements belong. Alternatively an independent mapping between the electrical and the thermal domain can be established where the electrical resistance heat is

directly accounted for in the thermal domain.

With this model one could also account for the change in resistivity of the current collectors due at different temperatures of the battery. There can be a great variation in the resistance of the current collectors at extreme temperatures which could affect the current and voltage distribution of the cell, and hence the safety and aging of the cell, significantly.

6.3 Conclusion

The electrical network model helps us develop a deeper understanding about lithium ion battery design with respect to their safety and aging. This is a unique model that accounts for the electrical domain in a lithium ion battery. The thermal, electrochemical and electrical models are developed independently and an efficient and accurate mapping methodology is developed to integrate these domains.

This model provides an important cell design tool. It gives an insight into how the tabbing arrangements can influence impedance and SOC distributions. This assists in understanding the aging of the cell. Current collector designs and their thicknesses influence the tradeoff between power and energy densities of the cell.

This model also helps us understand the safety tradeoffs at different charging rates. Fast charging strategies should account for the current collector designs. Li-plating driving force is high (varies by ~10mV) during a 2C charging of the energy cell when the current collector resistance is accounted for. Tabbing arrangements also influence this driving force in low-

resistance cells.

Thus, the electrical network is an important tool that assists in lithium ion battery designs. This can be expanded to other cell formats (prismatic), to make it more widely applicable.

Appendix A

Parameters in a current collector element:

Area

The area of a current collector element is the cross sectional area of the current collector along the current collector spiral, it is the thickness of the current collector (H^{NCC} or H^{PCC}) times the height of the cell in z-direction (z). It is in m^2.

Current

The current through the current collector element, measured in amperes (A).

DF_ID

DF_ID is the electrochemical element index to which the current collector segment belongs. A current collector element belongs to an electrochemical element if its centroid is located inside the particular element.

Length

The length of the current collector segment is the distance from one voltage point to the next. It is the arc length of the spiral segment between two consecutive voltage points, in meters (m).

$r_{Centroid}$

r_centroid is the distance of the mid point of the current collector from the center of the cell.

radial_distance

radial_distance is the distance of the start of the current collector from the center of the spiral, in meters (m)

resistance

Resistance is total resistance of the current collector, given by $\frac{\rho l}{A}$ (resistivity ρ, length l and cross sectional area A), in ohms (Ω)

θ

Theta is the angular distance of the start of the current collector.

$\Theta_{Centroid}$

$\Theta_{Centroid}$ is the angular distance of the midpoint of the current collector.

$Z_{Centroid}$

$Z_{Centroid}$ is the distance of the midpoint of the current collector in the z-direction.

Parameters of an electrical network element:

Area (A_k)

The area is an electric network element is the length of the electrical network element (measured through the separators) times the height of the cell (Z).

DF_ID

DF_ID is the electrochemical element index to which this electric network element belongs. If the centroid of the electrical network element is in the electrochemical element zone, the electrical network element belongs to that electrochemical element.

I_{new}, I_{old}

These are the currents through the separator from one current collector to the other in an electrical network element. I_{new} is the current in the present timestep and I_{old} is the current in the previous timestep.

L_N, L_P

These are the lengths of the negative and the positive current collector that is in the element. They are calculated such that the voltage nodes are in the middle of these current collector segments

neg_elem

neg_elem is the negative current collector element that belongs to the electrical network element

pos_elem

pos_elem is the positive current collector element that belongs to the electrical network element

$r_{Centroid}$

This is the radial distance of the centroid of the electrical network element. It is defined as half the sum of the radial distance for the negative and positive voltage points of this element.

S_{ID}

Separator ID. The separator ID of the electrical network tells if the element belongs to separator 1 or separator 2.

$Self_{ID}$

self_ID is the Index of the Electrical network element

SOC_{old}, SOC_{new}

These are the state-of-charge of the electrical network element. SOC_{new} is the state-of-charge in the present timestep and SOC_{old} is the state-of-charge in the previous timestep.

$\Theta_{Centroid}$

This is the angular distance of the centroid of the electrical network element. It has the same value as the angles of the positive and negative voltage nodes of that element

$V_{N,new}$, $V_{N,old}$, $V_{P,new}$, $V_{P,old}$

These are the voltages at the negative and positive voltage nodes of the electrical network elements. The 'old' voltages are from the previous timestep whereas the 'new voltages are from the present timestep.

volume

This represents the volume of the electrical network element. This would be used later on to calculate the heat generation in this element.